Karlsruhe Institute of Technology

A Model-Based Study on the Influence of Solar Activity on the Atmospheric Chemistry of Venus and Mars

Master thesis
by

Chiara Schleif

Department of Chemistry and Biosciences
Institute of Physical Chemistry
Molecular Physical Chemistry Group

Reviewer:	Prof. Dr. Matthias Olzmann
Second Reviewer:	Prof. Dr. Willem M. Klopper

01.02.2024 – 30.07.2024

Statutory Declaration

I declare that I have authored this thesis independently, that I have not used other than the declared sources / resources, that I have explicitly marked all material which has been quoted either literally or by content from the used sources and that I considered the KIT statutes for ensuring good scientific practice in the currently valid version.
Furthermore, I certify that the results used in the work were obtained within the period of time specified by the Examination Board.

Eidesstattliche Erklärung

Ich versichere wahrheitsgemäß, die Arbeit selbstständig verfasst, alle benutzten Hilfsmittel vollständig und genau angegeben und alles kenntlich gemacht zu haben, was aus Arbeiten Anderer unverändert oder mit Abänderungen entnommen wurde sowie die Satzung des KIT zur Sicherung guter wissenschaftlicher Praxis in der jeweils gültigen Fassung beachtet zu haben. Darüber hinaus versichere ich, dass die in der Arbeit verwendeten Ergebnisse in dem vom Prüfungsausschuss festgelegten Zeitraum der Arbeit entstanden sind.

Karlsruhe, _____

Date/Datum Chiara Schleif

Abstract

In this thesis, the influence of a Solar Particle Event (SPE) on the atmospheric chemistry of Venus and Mars, similar to the great Halloween Storms of 2003, has been investigated. For this, the ion chemistry model ExoTIC has been used, which is an atmospheric one-dimensional stacked box model. It considers a wide range of neutral, photolytic and ion chemistry reactions, with the latter being used for simulating the impact of charged particle streams on the atmospheric composition through ionisation, dissociation and dissociative ionisation of the components depending on altitude and ion fluxes.

The focus of this work is on the changes in the behaviour of the catalytic cycles that are assumed to be responsible for the observed CO_2 stability in the atmospheres of the two planets. Within these cycles, reactive species acting as catalysts enable an effective oxidation of CO by O_2 and O, among them HOx and NOx which are known to be produced in significant quantities on Earth during Solar Particle Events. For both planets, the event simulation revealed a significant production of HOx and NOx, with the abundance of NOx increasing by several orders of magnitude and that of HOx by only $\sim$5 and $\sim$25 percent, respectively. In correlation to that, an excess production of CO_2 during the event was simulated which could be explained by the combined effects of enhancements of several different catalytic cycles, mainly involving HOx as catalytic species. For Mars, an additional connection could be made between the changes in CO/CO_2 and O_2 and their relation to the diurnal cycle, which enabled to clearly identify the dominant catalytic cycles and their respective contributions.

Contents

1. Introduction

It is known that the Sun is not quiet but releases a continuous stream of charged particles, the so-called solar wind. It extends far into interplanetary space, reaching the planets and interacting with their magnetospheres. But aside from this always-present outflow, there are extreme events like Coronal Mass Ejections (CMEs) causing dense, high-energetic particle fluxes that can hit the planets and deeply penetrate the magnetospheres. The precipitating particles can reach lower atmospheric layers, resulting in a complex cascade of primary ion- and neutral follow-up reactions which can have major impacts on the atmospheric composition and its dynamics. On Earth it has been shown that this causes a significant production of reactive HOx (H, OH and HO_2) and NOx (N, NO and NO_2) species which are known to play important roles in several catalytic cycles, e.g., of stratospheric ozone destruction.

Based on these findings, the following question arises: What are the effects of such events in other planetary atmospheres with different compositions? This question is particularly relevant for exoplanetary research, as atmospheric measurements of transiting exoplanets are crucial to obtain detailed information about their characteristics. [1] To know how the composition of an atmosphere might be influenced by its host star is important for interpreting the observed spectra and to estimate the planets habitability, especially if the star is very active or the exoplanetary orbit is very close (which is for example both the case in the TRAPPIST-1 system [2]). To improve our knowledge on different types of atmospheres, the first step is to consider the closest and best known alternatives: our immediate neighbours Venus and Mars. Although both have CO_2-dominated atmospheres, these contain strikingly different atmospheric trace gases. Combined with their different physical parameters, including surface pressure, temperature profile, distance from the Sun and solar day length, this creates two very unique systems that are very different from Earth. As it is currently not possible to directly measure the impacts of a solar particle event in the respective atmospheres, simulations need to be done to assess short- and longer term effects on their neutral atmospheric composition and the chemical processes within.

2. Theoretical background

2.1 Space weather

The term space weather in general refers to the effects solar activity and other cosmic energy sources have on the Earths environment but also the rest of interplanetary space. [3] The following sections provide an insight into some of the most relevant phenomena and their impacts on the terrestrial magnetosphere and the atmospheric layers beneath.

2.1.1 Solar activity and space weather phenomena

The solar atmosphere consists of several layers called the Photosphere, Chromosphere and Corona. Their structures and dynamics are controlled by the magnetic field lines flowing through the layers, forming loops, twisted patterns and other complex structures. On the surface of the Corona, the outermost and at the same time hottest part of the atmosphere, darker spots that are referred to as coronal holes can be observed. Their abundance and size are correlated to the solar cycle, increasing significantly around solar maximum. These holes are featured by open magnetic field lines streaming into interplanetary space, enabling a continuous outflow of charged particles. This always-present phenomenon is called the solar wind, which drags the solar magnetic field outwards through interplanetary space (forming the interplanetary magnetic field, short IMF) and reaches the planets of the solar system. It consists mostly of H^+ and He^+ ions, as well a corresponding amount of electrons; their energies lie in the range of a few keV. Depending on its properties, especially the orientation of the IMF, the solar wind can interact with the magnetospheres of the planets, causing phenomena like aurorae, which can be observed not only on Earth but on other planets, too. Besides this always present particle stream, there are other, more extreme events that occur in context of space weather which can have major impacts on solar system bodies. Two relevant examples are Coronal Mass Ejections (CMEs) and solar flares, which are assumed to be the major sources of Solar Energetic Particles (SEPs). SEPs are characterised by intense proton (and electron) fluxes with energies up to several MeV, sometimes hundreds of MeV or even GeV, exceeding the solar wind by many orders of magnitude. CMEs are often caused by sudden eruptions of prominences

and sometimes correlated to a solar flare, pushing great amounts of energetic particles into the solar wind and therefore the interplanetary space. The resulting particle fluxes can highly vary in speed, where the fast ones can get accelerated to very high energies and propagate faster than the ambient solar wind; this causes its compression and the formation of a shock wave which travels through the interplanetary space and hits the planetary magnetospheres. Such a phenomenon can also be caused by the occurrence of high-speed solar wind, so-called co-rotating interaction regions, but as this work is focusing on Solar Particle Events (SPEs), this will not be explained further.
Depending on the magnetic properties, the interaction can result in minor to major disturbances where the particle stream penetrates not only the magnetosphere, but also the ionosphere and possibly even deeper atmospheric layers. There, the energetic particles can interact with the atmospheric constituents which may lead to temporal changes in the atmospheric composition.
This chapter is based on information taken from the literature [3] and [4].

2.1.2 Impacts of Solar Particle Events on Earth atmosphere

It has been shown that SPEs can cause significant changes in the abundances of odd hydrogen (HOx = H, OH, HO_2) and odd nitrogen (NOx = N, NO, NO_2) in altitudes ranging from the upper stratosphere to the lower thermosphere. [5] The lower thermosphere is located between 90-150 km, the upper stratosphere around 40 km, which corresponds to a pressure range of $< 10^{-2} - 10^{1}$ hPa; in between the two layers lies the mesosphere. [6]
Depending on the location and species, the changes can persist for longer time spans which causes long term effects and enables a downward transport of the produced species into lower atmospheric layers. This is particularly relevant for NOx which survives much longer than HOx due to its lower reactivity. The problem with this is that especially NOx serves as an effective catalyst in catalytic cycles concerning ozone loss in the stratosphere and can therefore cause an enhancement in ozone destruction in these altitudes, where also the lifesaving ozone layer is located. [5]
SPEs can have further effects beside the ones described above, e.g., on temperature behaviour and atmospheric dynamics, which will not be explained here in further detail but can be read up in Sinnhuber et al. [5]

2.1.2.1 Effects on the HOx budget

HOx is produced from atmospheric water vapor assuming that one H_2O molecule forms exactly H + OH per ion pair (a short explanation of the unit "per ion pair": formation rates of neutral species due to atmospheric ionization are commonly given relative to the rate of ion pair production). This does not happen directly but instead through the formation

and recombination of water-bearing cluster ions, which will not be explained in further detail here. The HOx-formation is expected to be most efficient in the middle and lower mesosphere as well as in the stratosphere, but not at higher altitudes, since the formation of H_2O cluster ions does not really occur there. Due to further reactions that will not be explained here, the ratio of OH:H is not exactly 1:1 but lower. More details on HOx can be read up in Sinnhuber et al. [5]
Atmospheric measurements have shown direct evidence for an increase in mesospheric OH as well as in stratospheric H_2O_2 and HO_2 due to an event. An increase of HOCl during the great Halloween storms of 2003 served as an indirect evidence for an increase of stratospheric HOx. [5] As the HOx species are very reactive, actually measuring the changes in their abundances is difficult, but simulations predicted an enhancement in mesospheric OH of over 100% and in stratospheric OH of over 10% for the great Halloween Storms. [7]

2.1.2.2 Effects on the NOx budget

Atomic nitrogen N can either be produced directly through dissociation, caused by the precipitating charged particles, or through follow-up reactions of reactive species that were formed through ionisation, dissociation and dissociative ionisation of N_2 and O_2. The latter are also responsible for the production of NO, which in turn produces NO_2. In short words the effective NOx production is a combination of direct ion reactions and indirect follow-up reactions. [8]
For the production of NO, the subsequent reactions are

$$N + O_2 \rightarrow NO + O \tag{2.1}$$

$$N + O_3 \rightarrow NO + O_2 \tag{2.2}$$

where N can either be in ground- or excited state. Besides the production, atomic N is also responsible for the destruction of NO, which is why the previous and the following reaction compete with each other:

$$N(^4S) + NO \rightarrow N_2 + O \tag{2.3}$$

Which reaction is dominating depends on temperature and abundances; at sufficiently low temperatures a high amount of $N(^4S)$ (like it is produced during SPEs) causes a net destruction of NOx. [5, 8]
For the great Halloween storms in 2003, an increase of NOx by a factor of up to 100 has been measured in the middle to upper mesosphere during the event while an increase by a factor of over 20 in the lower mesosphere has been observed for several days. This shows the strong and particularly longer lasting effect such SPEs can have on the NOx budget

of the terrestrial atmosphere. [7] The impact of NOx on ozone mentioned above has been shown to be latitude-dependant, being most relevant in the polar region; NOx that is produced above 80 km in the polar vortex causes ozone destruction in lower altitudes there due to effective down transport. [5]
Enhancements of NO around 70-85 and above 80 km during energetic electron precipitation events have served as an evidence for the correlation between the two incidents for the given altitudes, but no similar impact could be proofed in lower altitudes. In general it is still unsolved whether electron precipitation has a similar impact on stratosphere and mesosphere as large SPEs do, but if this is the case, the effects might be significantly smaller. [5]

2.2 Venus and Mars

The purpose of this chapter is the description of relevant characteristics and significant differences of Venus and Mars, also in comparison to Earth, in order to prepare the reader for the subsequent explanation of the simulations and analysis of the results.

2.2.1 Physical parameters

A comparison of the thermal structures of the atmospheres of Earth, Venus and Mars is shown in figure 2.1. Since the simulations are restricted up to 120 km for Venus and 85 km for Mars as will be explained later in the respective chapters, only the respective heights are relevant in this scheme. As can be seen, the atmospheric layers of Venus and Mars extend over much wider height ranges as they do on Earth, but since Mars is missing a stratosphere, its mesosphere is located in a similar altitude. For Venus (which is missing a stratosphere, too), both layers are shifted to slightly higher altitudes compared to Mars. The missing stratospheres are attributed to the absence of an ozone layer which is responsible for the radiant heating in the terrestrial atmosphere that in turn forms its stratospheric layer. The end of the troposphere, also called tropopause, is located on Venus at the level of its visible cloud layer which therefore serves as a separator between troposphere and stratosphere. Other striking differences are the surface temperatures and pressures, which are both highest on Venus. The former due to the much more intense greenhouse effect, the latter due to the very high atmospheric density, which results in a surface pressure almost 15,000 times greater than on Mars. Around 100 km, Earth and Venus show a similar temperature behaviour despite Venus being far closer to the Sun, while Mars is substantially colder. This is explained by the high CO_2 abundance, which serves as an effective cooling agent in thin atmospheres. [4]

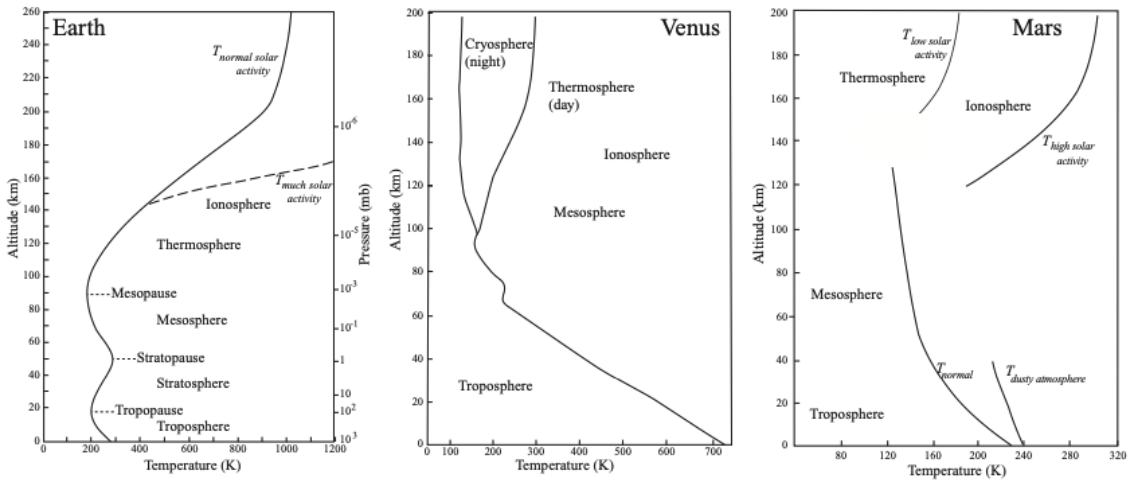

Figure 2.1: Schematical presentation of the thermal structures of Earth, Venus and Mars, taken from [4].

Other physical parameters of interest are summarised in table 2.1 and will be further explained in the upcoming subsections.

Table 2.1: Overview of the relevant physical parameters for Earth, Mars and Venus, taken from the NASA fact sheets if not explicitly mentioned else wise. [9]

	Earth	**Mars**	**Venus**
radius [km]	6378.1	3396.2	6051.8
orbital semi-major axis [AU]	1	1.524	0.72
solar day length [h]	24	24.66	2802.0
surface pressure	1.013 bar	6.36 mbar	92 bar
pressure scale height at surface [km]	8.34	11.1	15.9
mean surface T [K] [10]	288	220	730
bond albedo	0.294	0.25	0.77

2.2.1.1 Mars

The main constituents of the martian atmosphere are CO_2 and N_2, followed by several important trace gases like O_2, CO and H_2O. Therefore, its composition is strikingly different compared to the terrestrial atmosphere which mainly consists of N_2 and O_2. More details on the atmospheric components are given in section 2.2.2.1. Although Mars has a very thin atmosphere with a surface pressure of only 6.1 mbar which is reached on Earth around 40 km altitude, the two planets show a similar pressure around 100 km. This is explained by the lower surface gravity, which causes less change in pressure with altitude. Below the mesopause, the martian atmosphere is separated into middle ($\sim$ 50-100 km) and lower atmosphere, with the boundary height greatly varying with season, dust opacity and latitude. The changes in opacity are due to reoccurring dust storms which elevate surface particles into the atmosphere. [11] It is furthermore assumed that these storms may play an important role in heterogeneous atmospheric reactions, but this will not be taken into

account in the framework of this thesis and therefore not explained further.
Similar to Earth, Mars has a solar day length of 24.66 hours, resulting in a comparable diurnal cycle.

2.2.1.2 Venus

Venus is the planet of the solar system nearest to the Sun that contains an atmosphere, therefore the incoming solar radiation is almost twice as high as on Earth. Its atmosphere is approximately 100 times more massive than the terrestrial one and consists, like the martian atmosphere, mainly of CO_2 (and is therefore also strikingly different compared to Earth). These conditions combined favor the very strong greenhouse effect that is observed on Venus and which causes the surface temperature to reach values around 730 K. [12] One striking characteristic is the thick cloud layer extending from around 47-70 km, separating lower and upper atmosphere (with some additional hazes in lower and higher altitudes). The clouds consist mainly of condensed H_2SO_4 with some additional trace components, but its exact composition is still unsolved. The layer is so thick that it is basically opaque for UV, visible and most infrared wavelengths, which makes observations of the lower atmosphere and the surface difficult. [4] Due to the lack of radiation reaching the lower altitudes, it is assumed that the chemical processes there are driven mainly thermally, while the upper atmosphere is dominated by photolytic reactions. [12]
While Earth and Mars have similar solar day lengths, a venusian day is about 116 times longer with 2802 hours per day, resulting in a very long diurnal cycle.

2.2.2 Atmospheric compositions

Although both Venus and Mars contain a CO_2-dominated atmosphere, they show significant differences in their minor components, which results in diverging chemical processes and dynamics. The most striking differences concern the much lower mixing ratios of H_2 and H_2O on Venus, which in turn contains significant amounts of sulfur and chlorine species. An overview of the most important atmospheric constituents and their abundances is shown and further explained in the following subsections.

2.2.2.1 Mars

The average volume mixing ratios listed in table 2.2 were obtained by spacecraft- and ground-based measurements as well as analysis of *in situ* samples taken by the Viking lander and the Mars Science Laboratory mass spectrometer. CO_2, the major constituent of the martian atmosphere, experiences a large annual variation of up to 30% due to condensation and sublimation on and from the seasonal ice cups of the poles. Together with H_2O, it furthermore condenses in thin ice clouds during winter season; these changes in

abundances cause a variation of the other atmospheric abundances, too. Molecular oxygen O_2 has been difficult to detect in the martian atmosphere, which is why its abundance and seasonal variation is not fully resolved yet. The photolysis of CO_2 and H_2O are the major sources of O_2, since the produced atomic oxygen rapidly recombines to form O_2. CO, an important component for maintaining the photochemical cycle of CO_2 (see chapter 2.2.3), shows clear seasonal and latitudinal variations and is used for obtaining the thermal structure of the atmosphere. Ozone shows similar seasonal and spatial variations, forming two ozone layers in lower (30 km) and higher altitudes (30-60 km, highly variable). Their occurrence is seasonal, so the lower layer does only form during aphelion season when Mars is furthest away from the Sun, as observed by the SPICAM/UV instrument. [13] H_2O_2 is another variable component with a short lifetime which serves as a temporal HOx reservoir and plays an important role in the catalytic cycles for CO_2 stability. Molecular hydrogen H_2 is produced by H_2O-photolysis through reaction of H + HO_2, especially in 20-50km altitude. [11]

Table 2.2: Overview of the abundances in the martian atmosphere, ordered from highest to lowest. Since the most constituents show more or less extensive variabilities, the given values represent annual averages. [11]

constituents	CO_2[1]	N_2[1]	O_2[1]	CO[2]	H_2O[2]
average volume mixing ratio	0.9532	0.019-0.027	0.0012-0.0014	300-1600 ppm	15-1500 ppm
constituents	H_2[4]	O_3[2]	H_2O_2[3]	CH_4[1]	noble gases[1,2] (Ar, Kr, Xe)
average volume mixing ratio	17 ppm	10-350 ppb	0-40ppb	0.7-7 ppb	0.016-0.019

[1] measured by e.g. Curiosity rover / SAM [14, 15]
[2] measured by e.g. ESA Mars Express / PFS, SPICAM [16–18]
[3] measured by e.g. IRTF / TEXES [19]
[4] measured by FUSE [20]

In the quiet martian atmosphere, NOx species are only produced in the upper atmosphere due to the high energy that is needed to break the N_2-bond. Above 120 km, this energy is provided by extreme UV or energetic electrons resulting from photoionisation of other atmospheric components. In contrast to Earth, NO is produced through the reaction of $N(^2D)$ with CO_2:

$$N(^2D) + CO_2 \rightarrow NO + CO \tag{2.4}$$

the fast recombination

$$N + NO \rightarrow N_2 + O \tag{2.3}$$

that has already been mentioned in the context of Earth (see section 2.1.2) serves as an effective net sink of N and NO and together with the photolysis of NO, it results in N dominating the downward flux of NOx to lower altitudes. There, N quickly reacts with HO_2 form NO,

$$N + HO_2 \rightarrow NO + OH \tag{2.5}$$

which in turn limits NOx to low abundances due to reaction (2.3). But up to now, the nitrogen chemistry on Mars is still not sufficiently supported by actual measurements, detailed 3D models and kinetic data for a complete estimation of its relevance in the martian atmosphere. [11]

2.2.2.2 Venus

In table 2.3, the mean abundances as well as the latest height-resolved observational data of the upper atmosphere are listed for relevant species. The latter are described by discrete measurement points (even if continuous height profiles are available) because these are later used for comparison with the model simulations of the undisturbed atmosphere. Similar to Mars, the detection of O_2 above the clouds has not been successful yet, which is why the results of the latest 3D model from Stolzenbach et al. [21] are shown in table 2.3. They predict a maximum abundance of 180 ppm around 90 km and a genereal minimum background level of 20 ppm. The calculated upper limit above 58 km is 3 ppm, based on ground-based measurements with the HRF spectrometer. The model overpredicts that, which seems to be a general, still unsolved problem in all chemical models of the venusian atmosphere that have been published in the past. [21]

Ground- and spacecraft-based measurements of CO show its strong variability (especially above 90 km), which seems to be caused by a complex interplay of several processes. [22] In general, CO increases with altitude due to efficient CO_2-photolysis.

H_2O is observed to show no variation with altitude above the clouds, having a mean abundance of 1-2 ppm as measured by SPICAV and SOIR.

Ozone has only been measured on the night side of Venus by SPICAV-UV, which detected abundances down to 85 km. The values listed in table 2.3 do not show mean abundances but rather observed peak values.

For HCl, the spacecraft- and ground-based measurements are in a strong disagreement: the former show an increase with altitude from 70 km upwards, while the latter observed the opposite. This discrepancy is up to now still unexplained.

ClO, like O_3, has only been observed at night, where it seems to increase with altitude. The model from [21] predicts an opposite behavior during daytime with values one magnitude smaller.

Both SO and SO_2 show strong, similar diurnal variations which indicate a photochemical

Table 2.3: Overview of the abundances in the atmosphere of Venus. The first row shows the average volume mixing ratios (vmr) listed in [12] (if not marked otherwise), the second row the height resolved values for the upper atmosphere. the measurements of these were taken from [21], where Stolzenbach et al. used them for extensive comparison with their PCM model. The respective measuring techniques used by the original literature are mentioned in the footnotes of this table.

Components	CO_2	N_2	O_2	CO	H_2O
average vmr	0.965	0.035	$<$ 300 ppb (cloud tops)	4.5×10^{-5} (70 km) 1×10^{-3} (100 km)	60 ppm
height resolved vmr	/	n.a.	10 ppm (70 km)[(1)] 180 ppm (90 km)[(1)] 100 ppm (95 km)[(1)]	20 to 300 ppm[(2)] 60 to 300 ppm[(3)]	1-2 ppm [(3)]

Components	H_2	O_3	H_2O_2	HCl	noble gases (Ar, Kr, Xe)
average vmr	n.a.	(9.4-11.4)±4 ppb [21]	n.a.	6×10^{-7} (cloud tops)	70 ppm (Ar) 12 ppm (He) 7 ppm (Ne) 25 ppb (Kr) 1.9 ppb (Xe)
height resolved vmr	n.a.	nightside:[(3)] 1-30 ppb (85-90 km) 6-120 ppb (100-105 km)	n.a.	400 ppb (70km) $<$ 100 ppb (90km)[(2)] 40ppb (70km) 300ppb (90km) [(3)]	n.a.

Components	CH_4	ClO	SO	SO_2	H_2SO_4
average vmr	n.a.	nightside: [21] 2.6 ± 0.6 ppb	20 ppb	5-100 ppb	n.a.
height resolved vmr	n.a.	night side: 0.45-2.4 ppb (84-90 km);[(2)] dayside: 0.5-0.01 ppb (70-90 km)[(1)]	disk-averaged: 4-10 ppb (84-94 km)[(2)] 0.02-1 ppm (85-105 km)[(3)]	0.2-0.02 ppm (65-80 km); 0.05-2 ppm (85-105 km)[(3)]	determined upper limit: 3 ppb $>$ 85 km[(2)]

[(1)] PCM model [21]
[(2)] ground-based measurements from IRTF, JCMT or IRAM, details in [21]
[(3)] spacecraft-based measurements, mainly at terminator, from SPICAV or SOIR on-board Venus Express, details in [21]

correlation due to photolysis of SO_2 and recombination. In addition to that, they also exhibit non-diurnal changes and variations with latitude. [23] Both species increase with altitude, which stands in conflict with previous predictions and raised the assumption of a still unknown source in higher altitudes. [24] For SO_2, two mesospheric layers have been observed by Venus Express which are mentioned in table 2.3, where SO has only been measured in the upper layer. [23]
H_2SO_4 seems to only be significantly abundant in the gas phase below the clouds (which will not be relevant for this work), measurements with JCMT determined an upper limit of 3 ppb above 85 km.

2.2.3 Catalytic cycles for CO_2 stability

In a CO_2-dominated atmosphere, the main reaction that drives the photochemical processes is the photolysis of CO_2:

$$CO_2 \xrightarrow{h\nu} CO + O \tag{2.6}$$

The produced atomic oxygen recombines rapidly to form molecular oxygen, which competes with its photolysis

$$O + O \xrightarrow{M} O_2 \tag{2.7}$$

$$O_2 \xrightarrow{h\nu} 2\ O \tag{2.8}$$

The direct (thermal) reverse reaction of (2.6)

$$CO + O \xrightarrow{M} CO_2 \tag{2.9}$$

is spin forbidden and very slow. Considering only these four reactions to be responsible for the balance of CO_2, CO, O and O_2, one would expect significant amounts of both CO and O_2 and a ratio of $[CO]/[O_2] = 2$, but none of this is the case for Mars or Venus. Instead, ratios of 45 (Venus [12]) and 0.5 (Mars [11]) and low abundances of both species are observed. Therefore, effective reaction mechanisms are needed that enable fast CO_2 recovery and breaking the O_2 bond (especially for Venus) to explain the observed abundances. [4,12] Since Mars and Venus show striking differences in their minor components and atmospheric characteristics, the catalytic cycles assumed to contribute to the stability of CO_2 are not identical; as H_2O is much more abundant on Mars than on Venus, HOx species are expected to serve as the major catalysts there, while for Venus the sulfur and chlorine chemistry is assumed to play the dominating role. The respective cycles that were developed over the past half century will be explained in the following subsections.

2.2.3.1 Mars

This subsection is based on information taken from the literature [11], as it includes a very extensive description of all chemical processes that are currently known to happen in the martian atmosphere and is in agreement with other literature.
Besides CO_2, the photolysis of H_2O drives the photochemistry on Mars. Since the martian atmosphere is very thin, the UV-radiation needed for photolysis of the two can reach down to even the lowest atmospheric layers; therefore the interaction between the dissociation products dominates the chemical processes in the whole atmosphere.
It has been shown that the composition of the martian atmosphere is controlled by HOx species which are produced by the H_2O photolysis. Their catalytic behaviour enables reactions that are several orders of magnitudes faster than the direct recombination (2.9); which HOx species is driving the chemical cycles depends on the altitude: H dominates in the upper atmosphere, OH in the middle, HO_2 in the lower. In high altitudes, OH is rapidly transferred to O_2 by the reaction

$$OH + O \longrightarrow H + O_2 \tag{2.10}$$

due to high abundance of O through CO_2 photolysis, which is why HOx primarily consists of H up there. With decreasing height, the abundance of O decreases, too, which causes the reaction with CO to become the main reaction pathway for OH:

$$CO + OH \xrightarrow{M} CO_2 + H \tag{2.11}$$

The atomic hydrogen rapidly reacts with the abundant O_2 and forms HO_2, whereby the efficiency of this reaction increases with decreasing altitude, causing HO_2 to be the dominating HOx species in the lower atmosphere.

$$H + O_2 \xrightarrow{M} HO_2 \tag{2.12}$$

HO_2 in turn can quickly react with O from the CO_2 photolysis, which reproduces the OH that has been lost in the oxidation of CO:

$$HO_2 + O \xrightarrow{M} OH + O_2 \tag{2.13}$$

Therefore, the reactions (2.11), (2.12) and (2.13) together form the first catalytic cycle of the martian atmosphere, which will be referred to as "HOx cycle 1" from now on.

HOx cycle 1

This cycle is assumed to play the dominating role in CO_2 recovery, being responsible for approximately 85 % (according to chemical models, e.g., from Yung and Demore [25]). Its efficiency is depending on the availability of OH, so that the cycle is expected to be most effective in the middle atmosphere. As can be seen in the net reaction in figure 2.2, this cycle consumes atomic oxygen for the formation of CO_2.

HOx cycle 2

A lack of atomic oxygen causes HO_2 to preferably undergo a self-reaction instead of (2.13), which results in the formation of H_2O_2:

$$HO_2 + HO_2 \xrightarrow{(M)} H_2O_2 \tag{2.14}$$

H_2O_2 serves as a temporal HOx-reservoir (since its destruction is slower than the loss of HOx), especially in the lower atmosphere. Its photolysis recovers OH, which is approximately in balance with the formation during daytime. This results in a variation of the catalytic cycle 1 that is assumed to play a subordinate role (responsible for only $\sim 8\%$ of the CO_2 recovery). There are two major differences compared to cycle 1: firstly, it consumes O_2 instead of O for the oxidation of CO, secondly it is dependant on the diurnal cycle as it relies on the photolytic dissociation of H_2O_2.
In general, the HOx cycles are terminated when HOx is transferred to stable species, e.g., H_2O and H_2, which serve as an effective sink.

HOx cycle 1

$$H + O_2 \xrightarrow{M} HO_2 \quad (1)$$

$$HO_2 + O \xrightarrow{M} OH + O_2 \quad (2)$$

$$CO + OH \xrightarrow{M} CO_2 + H \quad (3)$$

net reaction: $CO + O \longrightarrow CO_2$

HOx cycle 2

$$2\ (H + O_2 \xrightarrow{M} HO_2) \quad (1)$$

$$HO_2 + HO_2 \longrightarrow H_2O_2 + O_2 \quad (4)$$

$$H_2O_2 \xrightarrow{h\nu} 2\ OH \quad (5)$$

$$2\ (CO + OH \xrightarrow{M} CO_2 + H) \quad (3)$$

net reaction: $2\ CO + O_2 \longrightarrow 2\ CO_2$

Figure 2.2: Overview of the HOx cycles considered for Mars. The labels were chosen for clarity in the analysis later in section 4.3.2.2.

As mentioned in section 2.2.2.1, the abundances of NOx are usually limited to very low values in the middle and lower atmosphere due to the downward flux of N exceeding that

of NO (or more general: there is no excess NO). In this case, NOx chemistry is assumed to play no significant role in the lower atmosphere. But this changes when NO gets more abundant than N, making it relevant for other atmospheric reactions than just (2.3), especially since the photolysis of NO is slow down there. The most important reactions considered here are:

$$NO + HO_2 \longrightarrow NO_2 + OH \tag{2.15}$$

$$NO_2 \xrightarrow{h\nu} NO + O \tag{2.16}$$

$$NO_2 + O \longrightarrow NO + O_2 \tag{2.17}$$

Different to NO, the photolysis of NO_2 is fast for visible wavelengths and therefore effective even in lower atmospheric layers. Taking into account these reactions leads to the formation of another two catalytic cycles, the NOx/HOx cylces 3a and 3b [25].

HOx/NOx cycle 3a and 3b

The two cycles both contain the same first and last step as the pure HOx cycles, but differ in the involved NOx reactions, as can be seen in figure 2.3: Cycle 3a shows a similar behaviour as cycle 2, as it also consumes molecular oxygen for the CO_2 recovery and is dependant on the diurnal cycle due to the photolytic dissociation of NO_2. Cycle 3b on the other hand is similar to cycle 1, since it has the same net reaction and is also independent from photolytic processes. According to model predictions (also e.g., from Yung and Demore [25]) , the coupled cycles are assumed to contribute 5-10 % to the CO_2 formation. They terminate, similar to the pure HOx cycles, when NO_2 is transferred to stable sinks, e.g., HNO_3, HO_2NO_2 or also N_2O_5.

HOx/NOx cycle 3a

$$2\ (H + O_2 \xrightarrow{M} HO_2) \quad (1)$$

$$NO + HO_2 \longrightarrow NO_2 + OH \quad (6)$$

$$NO_2 \xrightarrow{h\nu} NO + O \quad (7)$$

$$HO_2 + O \xrightarrow{M} OH + O_2 \quad (2)$$

$$2\ (CO + OH \xrightarrow{M} CO_2 + H) \quad (3)$$

net reaction: $2\ CO + O_2 \longrightarrow 2\ CO_2$

HOx/NOx cycle 3b

$$H + O_2 \xrightarrow{M} HO_2 \quad (1)$$

$$NO + HO_2 \longrightarrow NO_2 + OH \quad (6)$$

$$NO_2 + O \longrightarrow NO + O_2 \quad (8)$$

$$CO + OH \xrightarrow{M} CO_2 + H \quad (3)$$

net reaction: $CO + O \longrightarrow CO_2$

Figure 2.3: Overview of the HOx/NOx cycles considered for Mars. The labels were chosen for clarity in the analysis later in section 4.3.2.2.

2.2.3.2 Venus

The following section focuses explicitly on mechanisms relevant for the stratospheric chemistry as the simulations done in this work are restricted to the atmosphere above the cloud top and do not consider vertical transport, which makes the chemical processes below the clouds irrelevant. As Venus lacks sufficient H_2O and H_2 in the atmosphere to be expected to produce significant amounts of HOx, the efficiency of HOx cycles similar to the ones on Mars are being questioned [12], but will be discussed here anyways due to the known impact of SEPs on the terrestrial HOx budget (raising the assumption of a similar effect on other planets). As HOx acts as a catalyst, already low abundances additionally produced by an event might be sufficient to enhance the significance of HOx cycles. The two schemes, first considered by McElroy et al. [26] for the venusian atmosphere, are identical to the martian HOx cycles and shown again below in figure 2.4.

HOx cycle 1

$$\mathrm{H + O_2 \xrightarrow{M} HO_2} \quad (1)$$

$$\mathrm{HO_2 + O \xrightarrow{M} OH + O_2} \quad (2)$$

$$\mathrm{CO + OH \xrightarrow{M} CO_2 + H} \quad (3)$$

net reaction: $\mathrm{CO + O \longrightarrow CO_2}$

HOx cycle 2

$$\mathrm{2\ (H + O_2 \xrightarrow{M} HO_2)} \quad (1)$$

$$\mathrm{HO_2 + HO_2 \longrightarrow H_2O_2 + O_2} \quad (4)$$

$$\mathrm{H_2O_2 \xrightarrow{h\nu} 2\ OH} \quad (5)$$

$$\mathrm{2\ (CO + OH \xrightarrow{M} CO_2 + H)} \quad (3)$$

net reaction: $\mathrm{2\ CO + O_2 \longrightarrow 2\ CO_2}$

Figure 2.4: Overview of the HOx cycles considered for Venus. The labels were chosen for clarity in the analysis later in section 5.4.2.2.

Chlorine-catalysed cycles

Due to the discovery of SO_2 and HCl in the upper atmosphere, the roles of ClOx and SOx as catalytic species for the oxidation of CO gained interest. Yung and DeMore [27] considered (among others) the following mechanism:

$$\mathrm{Cl + CO \xrightarrow{M} ClCO} \quad (2.18)$$

$$\mathrm{ClCO + O_2 \xrightarrow{M} ClCO_3} \quad (2.19)$$

$$\mathrm{ClCO_3 + Cl \longrightarrow Cl + CO_2 + ClO} \quad (2.20)$$

$$\mathrm{ClO + O \longrightarrow Cl + O_2} \quad (2.21)$$

net reaction: $\mathrm{CO + O \longrightarrow CO_2}$

The problem with this cycle is the missing explanation of the low O_2 abundance observed in the venusian atmosphere, since the net reaction only consumes atomic instead of molecular oxygen. This was solved with the discovery of the reaction between SO and ClO which eventually led to the formulation of a coupled SOx/ClOx cycle [12] which is shown on the right side. This mechanism shows similarities to the tropospheric CO oxidation cycle known from Earth despite using different catalytic species. Cycles with NOx and HOx as active species (as on Earth) could theoretically also play a supporting role on Venus, but only if there is sufficient NOx available. Lightning has been proposed as a possible source of NOx, so several scientist (Watson et al. [28], Chameides et al. [29]) examined in 1979 the potential role of NOx in CO_2 cycles. This led to the two reaction mechanisms shown in figure 2.5, one of them additionally coupling the oxidation of CO and SO_2.

SOx/ClOx cycle

$$SO_2 \xrightarrow{h\nu} SO + O \quad (6)$$

$$Cl + CO \xrightarrow{M} ClCO \quad (7)$$

$$ClCO + O_2 \xrightarrow{M} ClCO_3 \quad (8)$$

$$ClCO_3 + Cl \longrightarrow Cl + CO_2 + ClO \quad (9)$$

$$ClO + SO \longrightarrow Cl + SO_2 \quad (10)$$

net reaction: $CO + O_2 \longrightarrow CO_2 + O$

HOx/NOx cycle

$$2(H + O_2 \xrightarrow{M} HO_2) \quad (1)$$

$$HO_2 + NO \longrightarrow NO_2 + OH \quad (11)$$

$$NO_2 \xrightarrow{h\nu} NO + O \quad (12)$$

$$HO_2 + O \xrightarrow{M} OH + O_2 \quad (2)$$

$$2(CO + OH \xrightarrow{M} CO_2 + H) \quad (3)$$

net rct.: $2\ CO + O_2 \longrightarrow 2\ CO_2$

HOx/NOx/SOx cycle

$$H + O_2 \xrightarrow{M} HO_2 \quad (1)$$

$$HO_2 + NO \longrightarrow NO_2 + OH \quad (11)$$

$$NO_2 \xrightarrow{h\nu} NO + O \quad (12)$$

$$CO + OH \xrightarrow{M} CO_2 + H \quad (3)$$

$$SO_2 + O \xrightarrow{M} SO_3 \quad (13)$$

$$SO_3 + H_2O \xrightarrow{H_2O} +H_2SO_4 \quad (14)$$

net rct.: $CO + SO_2 + O_2 + H_2O \longrightarrow CO_2 + H_2SO_4$

Figure 2.5: Overview of the HOx/NOx cycle (left) and the HOx/NOx/SOx cycle with the latter coupling the oxidation of CO_2 and SO_2. The labels were chosen for clarity in the analysis later in section 5.4.2.2.

As it is known from Earth that SEPs can cause major changes in the NOx budget, these cycles gain interest against the background of investigating the impact of SEPs on the venusian atmosphere.

Yung and DeMore [27] did an extensive study of the venusian (photo)chemistry, compar-

ing different model set-ups which considered either HOx-, nitrogen or chlorine-dominated chemistry. Based on their results, they came to the conclusion that the chlorine-chemistry must play a significant role for the stability of CO_2, including the reactions (2.18)-(2.21). This assumption is still relevant today, although the thermal stability of ClCO, a central species in this chemical mechanism, might be lower than assumed by chemical models. This could result in a lower effectiveness of the ClOx-catalysed CO oxidation than previously predicted. [30]

2.2.3.3 Reaction mechanisms: rate-determining steps

The rate of the net reaction of a certain reaction mechanism is depending on the so-called rate-determining step. This step is considered as the slowest reaction in the sequence of elementary reactions that make up the reaction mechanism. When looking at an isolated mechanism the steady state approximation can be applied on, the comparison of the reaction rate constants is crucial in order to identify the rate-limiting step. The reason for that is that in steady state, the speeds of all steps are assumed to be identical as there is no net change in the abundances of the reactants and intermediates observed. [31] It is important to mention that only rate constants of the same reaction order can be compared, as the unit differs with the order; for reactions of (effective) second order, the unit is for example [cm^3/(molecule $\times$ s)]. [31]

In contrast to the given definition, the catalytic cycles considered in this thesis cannot be assumed isolated or in steady state, as they are included in a very complex chemical environment containing a lot of other simultaneously ongoing reactions and reaction mechanisms. Therefore, an analysis of the rate constants alone is not sufficient to obtain further information about the behaviour of the net reactions; instead it is favored to consider the reaction rates. However, an additional comparison of the rate constants might be performed if helpful for the analysis process.
Since it is assumed in the simulation that all reactions included (except the photolytic reactions) are of (effective) second order, the respective reaction rates are calculated as follows when considering a reaction of type A + B $\rightarrow$ C:

$$\frac{d[\mathrm{C}]}{dt} = k \times [\mathrm{A}] \times [\mathrm{B}] \tag{2.22}$$

This is mentioned in view of the analyses done in the subsequent chapters.

3. The model ExoTIC

The Exoplanetary Terrestrial Ion Chemistry model (ExoTIC) which was used in this work, is a 1D box model of the atmosphere, whose predecessor UBIC (University of Bremen Ion Chemistry Model) has originally been written for Earth but then got expanded to suit for any atmospheric composition. It considers a wide range of photolytic-, neutral- and ion reactions, with the neutral and the ion chemistry being treated separately, enabling the simulation of both the quiet and disturbed atmosphere. The ion chemistry is used to simulate the impact of charged particle fluxes from SEPs on the neutral atmospheric composition of the respective planet and will be further explained in section 3.2.

3.1 Neutral chemistry

The neutral chemistry module is based on the chemistry routines of SLIMCAT (from Chipperfield [32]) and serves as the superordinate model in which the zero-dimensional ion chemistry module can be embedded. [8] When UBIC got expanded to ExoTIC, the ability to calculate the time- and latitude dependant solar/stellar flux based on given orbital parameters and input spectra from the Sun or respective star was added. With this, ExoTIC can be used to also simulate exoplanetary atmospheres.

The one-dimensional character of the model is obtained by the stacked-boxed principle. Between the boxes, the model does not consider any type of transport except the radiative flux from top to bottom, which depends on the abundances of the absorbing species in every box. The neutral chemistry can be used without the ion chemistry module in order to simulate the calm atmosphere, e.g., for necessary reference calculations.

ExoTIC considers 60 neutral species in the case of Mars; for Venus there are 66 as the model was expanded by several species to simulate the chlorine and sulfur chemistry accordingly, which will be further explained in section 5.2. It includes around 160 reactions of neutrals (for Venus, the model was expanded by 14 further reactions within this thesis) where the respective reaction rates were taken from the JPL catalogue of 2006 [33]. The newly implemented reactions rely on the latest version from 2019 [34] when listed there, otherwise taken from other literature which is referenced accordingly in section 5.2. Furthermore, the model includes 49 photolysis reactions, expanded to 53 for Venus.

The initial atmosphere, from which the simulation starts, is passed to the model and contains 130 species as well as height-, temperature- and pressure profiles, from which a selection of relevant species is read in. This input dataset is calculated by the 1D chemistry-climate model 1DTERRA and provided by the group of Lee Grenfell from the DLR Adlershof; further details on its working methods can be found in Wunderlich et al. [35]. It has to be mentioned that, even when simulating a calm atmosphere, the compositions drift away from the initial values, since the models 1DTERRA and ExoTIC are not identical and therefore establish different dynamical equilibria. The most significant difference between the models is that 1DTERRA considers a global and temporal average for the photochemical equilibrium, while ExoTIC simulates time-dependent for one specific location. Hence, it is necessary to not start an event directly at the beginning of a simulation but instead after a spinup time of some hours or days, so that the calm atmosphere has enough time to equilibrate (as far as possible).

3.2 Ion chemistry

As the ion chemistry module that is embedded in ExoTIC is zero-dimensional, it needs to be called for each box of the 1D neutral chemistry model separately, resulting in a successive calculation of the ion chemistry from top to bottom in each time step before the calculation of the neutral chemistry. For each level, the following parameters are calculated in the appropriate order: first, the production- and loss rates of the reactants and products involved in the dissociation, ionisation and dissociative ionisation of N_2, O_2 and CO_2 are determined. Then, the ions, the electron density and the first exited state of N are brought to photochemical equilibrium, considering the rates calculated beforehand and the neutral atmospheric composition of the respective time step. Last, the resulting production- and loss rates of the neutral species, depending on the ion density reached in the photochemical equilibrium and again the neutral composition is calculated and handed over to the neutral chemistry.

During one time step, the composition and the ionisation rate are considered as constant due to the assumption of ionisation reactions being significantly faster than the neutral reactions. Inside the ion chemistry, the positive and negative ion chemistry are calculated separately to minimise computational effort. [8] In total, 160 charged species are considered for the simulation. Details on all ion reactions included in the ion chemistry model can be found in Sinnhuber et al. [5].

The ionisation rates used for the event simulation are provided by Konstantin Herbst from the University of Kiel, using the Atmospheric Radiation Interaction Simulator (AtRIS) to calculate the ionisation rates (caused by top-of-atmosphere particle fluxes) for the respective planetary atmospheres. For this, the same initial atmosphere as for ExoTIC has been

used (provided, as mentioned before, by the 1DTERRA model of Lee Grenfell). More details on AtRIS can be found in Herbst et al. [36].

3.3 The integration method

The integration is done after a semi-implicit method called SIS-scheme, which is short for semi implicit symmetric scheme and was developed by Ramaroson in 1989 [37]. It is a numerical method which can be used for solving stiff differential equations; here, the respective equations describe the temporal change of each species depending on all the reactions they participate in (through either loss or production). The integration scheme then calculates the approximate change of a species abundance per given time interval. [38] The rate of change for one species x_i is described as

$$\frac{d[x_i]}{dt} = f_i([x_1], ..., [x_N]) = P_i - L_i \tag{3.1}$$

where $[x_i]$ is the concentration of species x_i, and P_i and L_i are describing the production- and loss rates, respectively:

$$P_i = \sum_{j,m \neq i} k_{jm} \times [x_j] \times [x_m] + \sum_{m \neq i} j_m \times [x_m] \tag{3.2}$$

$$L_i = [x_i] \times \left(\sum_m k_{im} \times [x_m] + j_i \right) \tag{3.3}$$

k_{jm} are the rate constants of (pseudo-) bimolecular reactions producing i, k_{im} of reactions consuming i; j_m and j_i describe the photolysis rates. The equations (3.1) of all species are the stiff differential equations that need to be solved; in the SIS scheme, the concentration changes per timestep Δt are calculated approximately as follows:

$$\Delta \boldsymbol{x} = \boldsymbol{x}(t + \Delta t) - \boldsymbol{x}(t) \approx \frac{\Delta t}{2} \times \left[\boldsymbol{f}(\boldsymbol{x}(t + \Delta t)) + \boldsymbol{f}(\boldsymbol{x}(t)) \right] \tag{3.4}$$

$\boldsymbol{x}$ and $\boldsymbol{f}$ represent the tupel of all $[x_i]$ and f_i. Using the linear approximation

$$\boldsymbol{f}(\boldsymbol{x}(t + \Delta t)) \approx \boldsymbol{f}(\boldsymbol{x}(t)) + \left(\frac{d\boldsymbol{f}(\boldsymbol{x}(t))}{dt} \right) \times \Delta t \tag{3.5}$$

and the chain rule of derivation obtains

$$\Delta \boldsymbol{x} \approx \frac{\Delta t}{2} \times \left[2 \times \boldsymbol{f}(\boldsymbol{x}(t)) + \boldsymbol{J}_f \times \Delta \boldsymbol{x} \right] \tag{3.6}$$

$\boldsymbol{J}_f$ describes the Jacobian matrix of the function $\boldsymbol{f}$, which consists of the production and loss terms of all species previously described in the equations (3.2) and (3.3). [8, 38]

3.4 Utilisation in this work

In the framework of this thesis, ExoTIC has been used to simulate the influence of a SPE similar to the great Halloween Storms of 2003 on the atmospheric composition of Venus and Mars. For that, the proton and electron fluxes that have been measured on Earth during the event were scaled to the TOA (top of atmosphere) of the respective planets and used as input for the AtRIS model. This provided in turn the altitude-dependent atmospheric ionisation which was then used as input for ExoTIC.
To consider important processes regarding the sulfur and chlorine chemistry in the venusian atmosphere, the neutral chemistry model has been extended by a list of species and reactions which are further explained in chapter 5.2. The resulting impacts of the event are first compared to changes that are known to happen in the terrestrial atmosphere (previously described in chapter 2.1.2), followed by the analysis of the effects on the efficiencies of the catalytic cycles presented in chapter 2.2.3 in order to explain the observed variations in the abundances of CO, CO_2 and O_2.

4. Mars

4.1 Simulation setup

The total simulation time was 240 hours, which corresponds to approximately 10 martian days (named sols), as Earth and Mars both have almost the same day length (see table 2.1). Therefore, the diurnal cycle becomes relevant for this simulation, as photolysis is switched on and off accordingly.
Two types of simulations were made: a reference run independent from the event and an event run. The reference is needed to eliminate changes that are caused by the drift of the neutral atmosphere and the reoccurring diurnal changes. Further details on the event simulation are given in section 4.3. The calculations extended from the surface to 84 km altitude, which corresponds to a pressure range of 5.84 - 1.07×10^{-4} hPa and was defined by the input file that also contained the initial atmospheric composition. The location was set to 60° latitude, 0° longitude, the minimum solar zenith angle was therefore not zero but 60° as well. The simulations started at midnight at perihelion, which is defined as the point on orbit with minimum distance to the Sun. Heterogeneous chemistry was neglected, therefore no (ice) cloud formation was considered and all atmospheric components were in the gaseous phase at all times.

4.2 Simulating the quiet atmosphere

The abundances resulting after 234 hours (daytime) and 222 hours (night) from the reference simulation are compared to the available measurements that are listed in table 2.2. As these values are all average abundances for the whole atmosphere, they are included into the height profiles of the simulation results as rectangles (to mark an abundance-range) or vertical lines (if one certain value was given). Furthermore, the abundances that were provided by the input file are also added to the diagrams. This has two reasons: on the one hand it illustrates the atmospheric drift that has been mentioned above, on the other hand it explains some of the occurring under-predictions, as will be described in more detail in the subsequent paragraphs. Majority of the graphs can be viewed in the appendix in figure 7.1, but a short explanation on all is given below.

As can be seen, CO_2 is being under- and CO over-predicted in altitudes above 50 km, which corresponds to pressures below 1×10^{-2} hPa. This is most likely caused by a general overestimation of photolysis, probably by the Lyman-alpha line, as a similar pattern is observed for H_2O (and H_2O_2). In lower altitudes, the simulations are in relatively good agreement with the measurements, at least for CO_2, CO and H_2O_2. The comparison of CO is shown in figure 4.1. The volume mixing ratio of H_2O is massively underestimated from 10 km upwards, but it has to be mentioned that already the input file contained a H_2O abundance way below the measurements, as can be seen in figure 4.1. The case is similar for H_2O_2, although the initial values show less deviation from 50 km upwards than the final simulations, therefore the model either over-estimates the destruction of H_2O_2 (e.g., by photolysis) or under-estimates its production in the respective altitudes.
The simulations of N_2, H_2 and O_3 are in very good agreement with the measurements, O_2 is only slightly over-predicted and is still in the same order of magnitude, as can be seen in figure 4.1. Also NO lies within the upper limit determined by ground-based measurements [39], which is not listed in table 2.2 as it is just a limit and no certain abundance range. The slight under-prediction of CH_4 is also coming from the initial values, but it lies only half a magnitude below the lower limit. The noble gases were not compared as they are on the one hand not all contained in the model, on the other hand irrelevant for chemical processes anyway due to their inertness.

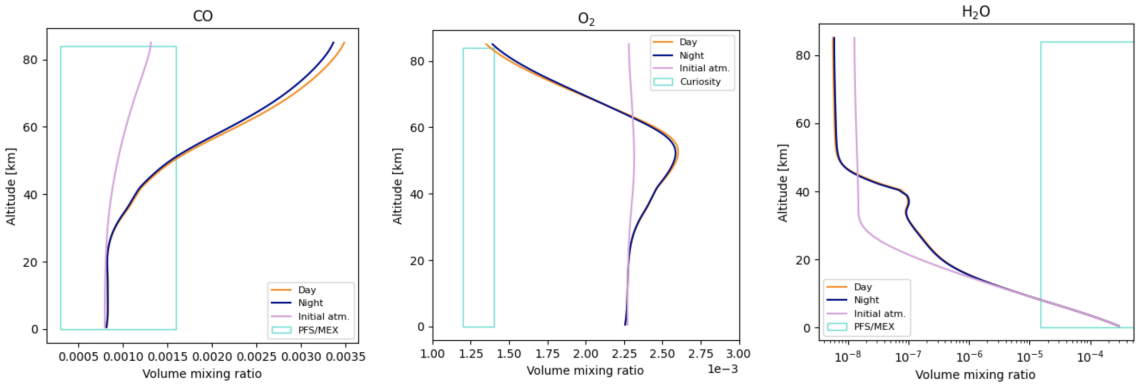

Figure 4.1: Comparison of simulation results and initial compositions with the available measurements for CO, O_2 and H_2O.

4.3 Simulation of the Solar Particle Event

For Mars, two event simulations were carried out, differing in the starting point of the event to evaluate the impact of the diurnal cycle on its course. The SPE always lasted for 24 hours, starting around midnight of day 6 (after 120 hours of simulating the quiet atmosphere) in the first run and around noon of day 6 (after 130 hours) in the second run. An overview of important time stamps is given in table 4.1. The event started several days after the begin of the simulation instead of immediately afterwards to ensure that

the changes in the neutral atmosphere per time step due to the drift described earlier are comparably small. At the same time, the starting point had to be chosen early enough to ensure there is sufficient time afterwards to observe the atmospheric response to the disturbance (referable to as "medium-term effects").

Table 4.1: Listing of the relevant simulation time stamps. As sols are slightly longer than terrestrial days, the time stamps have no round values.

	first run	**second run**
simulation period before perturbation	120 hours ($\sim$ 4.9 days)	130 hours ($\sim$ 5.3 days)
event start	hour 121 = midnight of day 6	hour 131 = before noon of day 6
event end	hour 144 = before midnight of day 7	hour 154 = before noon of day 7
simulation period after perturbation	96 hours ($\sim$ 3.9 days)	86 hours ($\sim$ 3.5 days)

4.3.1 Changes in NOx and HOx: Comparison to Earth

Although two major simulations have been made, the analysis will focus on the second event run, starting and ending at daytime, with additional comments on results of the first run (referred to as "night start" from now on) if they give supporting information. In general, the response of the HOx and NOx species to the event are similar in both simulations, but as their formation in the calm atmosphere is depending on the diurnal cycle, there are differences occurring due to the "coupling" of the effects of the diurnal cycle and the event. The following analysis will especially highlight the changes appearing in the pressure range of 5×10^{-2}-5×10^{-1} hPa (later referred to as "around 1×10^{-2} hPa") as this region shows the most significant $CO/CO_2/O_2$ changes, further discussed in section 4.3.2.1.
The changes observed in lower pressure ranges (at higher altitudes) are more or less irreversible over the time period that was given for atmospheric recovery, because collision reactions on the one hand are much less efficient due to the low density, photolytic dissociation on the other hand very fast due to the high solar irradiation. This serves as another reason why the upper heights will not be analysed in further detail.

4.3.1.1 Changes in the HOx budget

The temporal evolution of the HOx species relative to the reference atmosphere can be seen in figure 4.2. The blue colorbar refers to a deficit compared to the reference, the pink colorbar to a surplus. The corresponding plots for the night start can be found in the appendix in figure 7.3.

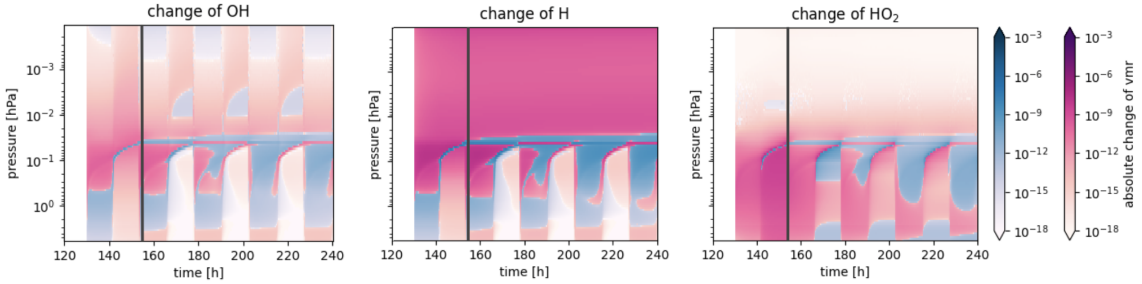

Figure 4.2: Contour plots of the changes in OH, H and HO_2 compared to the reference. Blue describes a deficit, pink a surplus in comparison to the calm atmosphere. The end of the event is marked with a grey line.

OH

Excess OH is produced over the course of the event around 10^{-1} hPa and upwards, with a relative change in the range of 25 %; destruction happens at lower layers during daytime, while at night, OH is produced in all layers. After the end of the event, the surplus remains and slowly starts to get destructed, running into a deficit during daytime after hour 200, which refers to sunrise on day 9. During nighttime, the surplus keeps reoccurring until the end of the simulation. In comparison to the observations made on Earth that have been described in section 2.1.2.1, the magnitude of change is within the same range.

H

H shows a behaviour according to OH, despite the changes above 5×10^{-2} hPa being independent of the diurnal cycle and the relative change being slightly lower, around 20 %. The similarity to OH is explained by their formation: Both are resulting from the destruction of H_2O; not only through photolysis but also by the ion chemistry caused by particle impacts. This can be seen in the mean production rates of the three species due to the positive and negative ion chemistry, shown in figure 4.3.

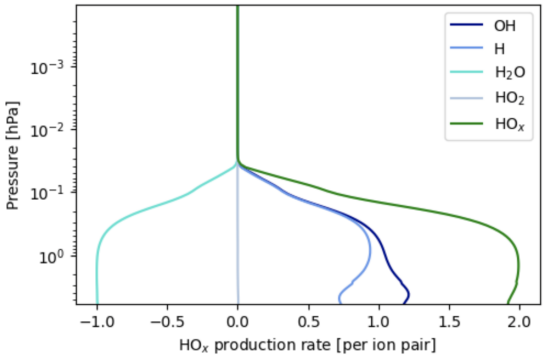

Figure 4.3: Mean production rates per ion pair of the HOx species (and H_2O). Due to the linear x-axis (to display negative values), the rates above 5×10^{-2} hPa appear to be ∼0; this is not the case; The production of HOx due to the event is in all layers >0, just several orders of magnitude bigger below 5×10^{-2} hPa.

HO_2

An excess production of HO_2 is happening in the whole atmosphere during the event, which remains afterwards until sunset of day 7 (∼hour 165). At the following day times, a growing area of deficit occurs; from sunrise of day 9 on, the pressure range of interest is in complete deficit. The deficit recovers each night, always turning into a continuous surplus again, with exception of the first night, where the area around 1×10^{-1} hPa shows a deficit. Although the produc-

tion rate of HO_2 through ion chemistry looks as if it is close to zero, it is not, but two orders of magnitude smaller than the rates from H and OH. HO_2 is produced as a further product of the H/OH production, which might be the major contribution to the observed increase. The corresponding neutral reactions are:

$$H + O_2 \xrightarrow{M} HO_2$$

$$OH + O_3 \longrightarrow HO_2 + O_2$$

$$OH + H_2O_2 \longrightarrow HO_2 + H_2O$$

However, they are competing with neutral loss reactions that are involving for example the other HOx species as well. As the abundance of HO_2 is usually rather low, its mean relative change lies in the range of 250 % during the event.

The surplus in HOx that is generated during the event (coming from H_2O) is afterwards quickly transferred into H_2O_2, which serves as a temporal reservoir and is in a strong surplus basically over the whole simulation; the respective line plot is shown together with H_2 and H_2O in figure 4.4. From there, it is gradually turned back into H_2O, which explains the slow recovery of H_2O that can be seen in the temporal evolution of its difference. At the same time, the excess of H_2O_2 decreases after the event and is almost completely regressed at the end of the simulation. However, this is not the case for H_2O, which is not fully being recovered. Instead, part of it transfers into H_2, which can be seen by comparing their temporal evolution: at the end of the simulation, the remaining deficit of H_2O corresponds to the observed surplus of H_2. As H, OH and HO_2 are very reactive species, their observed changes are several orders of magnitude lower than of H_2O, H_2O_2 and H_2, which in turn are significantly less sensitive to the diurnal cycle. Therefore, the overall long term transfer from H_2O over H_2O_2 to H_2 is not directly visible in the HOx species but only in the behaviour of the reservoirs.

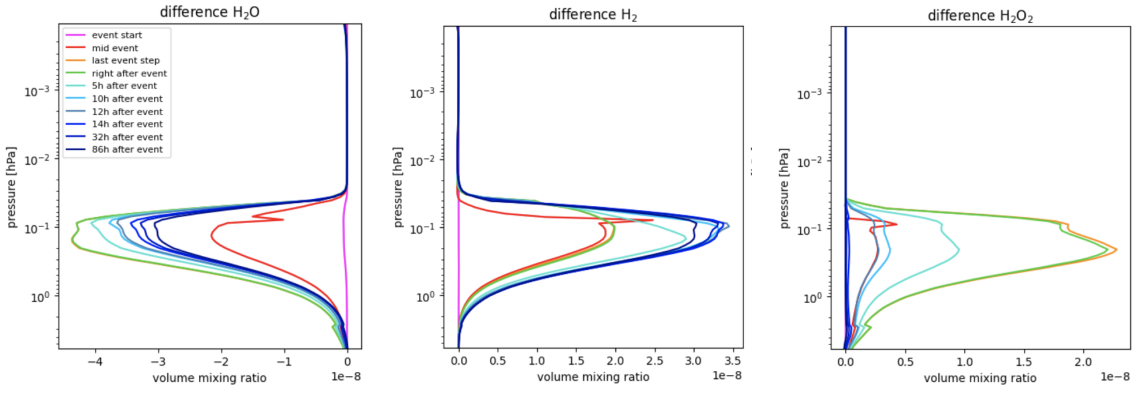

Figure 4.4: Temporal evolution of the differences of H_2O, H_2 and H_2O (event simulation compared to reference).

4.3.1.2 Changes in the NOx budget

During the event, NOx shows a similar behaviour to HOx as a surplus is being produced; but afterwards, the two species behave quite differently, which will be explained in more detail below. The contour plots of the differences of N, NO and NO_2 are displayed in figure 4.5. The relative change of all three NOx species is extremely high, in the range of $10^1 - 10^4$ %, since their abundances in the previously quiet atmosphere were very low.

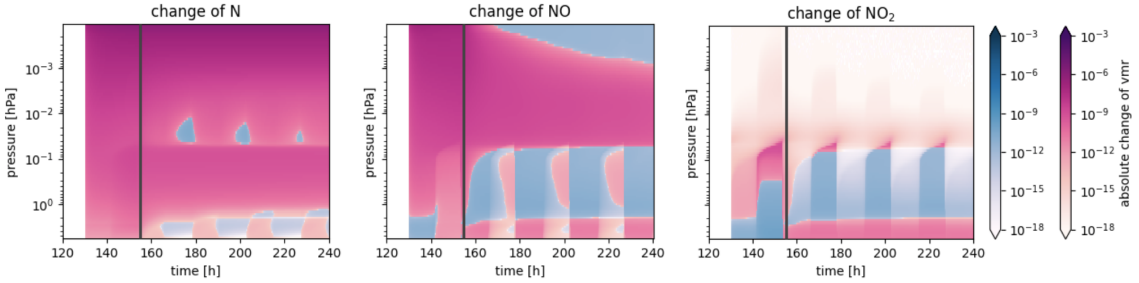

Figure 4.5: Contour plots of the changes in N, NO and NO_2 compared to the reference. Blue describes a deficit, pink a surplus in comparison to the calm atmosphere. The end of the event is marked with a grey line.

N

The great excess of N that is being produced during the event is explained by N_2 being the second most abundant component in the martian atmosphere and its effective destruction by the precipitating particles (as explained in section 2.1.2.2 for Earth). After the event, this strong surplus remains in 1×10^0-1×10^{-1} hPa and in higher levels for the rest of the simulation and decreases only very slowly. The reason for this is that the only relevant N_2 recovery reaction is

$$N(^4S) + NO \longrightarrow N_2 + O \tag{2.3}$$

and that N is much more abundant than any other NOx species.

NO

NO experiences a quick degradation of the previously produced surplus after the end of the event, turning into a deficit already a few hours afterwards. This is explained by reaction (2.3), as the strongly increased abundance of N enhances its rate and causes the occurrence of a NO deficit compared to the reference (since a higher excess of N than of NO is produced by the event). In addition to that, there are further reactions that consume NO and produce, e.g., NO_2. At night, the re-occurrence of a NO surplus can be observed, which could be explained by missing photolytic reactions, while the (enhanced) NO-forming reactions are continued:

$$N + O_2 \longrightarrow NO + O \tag{4.1}$$

$$N + O_3 \longrightarrow NO + O_2 \tag{4.2}$$

$$NO_2 + O \longrightarrow NO + O_2 \tag{4.3}$$

NO_2

NO_2 shows the same behaviour as NO, although its degradation partly starts already at night during the event. Almost directly after the event (5 hours), over the course of day 7, NO_2 runs into a deficit in 1×10^{0}-1×10^{-1} hPa, which remains for the rest of the simulation. The deficit compared to the reference is explained by the effective capture in NOx sinks: both NO_3 and N_2O_5 show a significant increase especially at night during the event which decreases again afterwards, HNO_3 however remains in its surplus and therefore seems to serve as an end sink of NOx. It is produced by

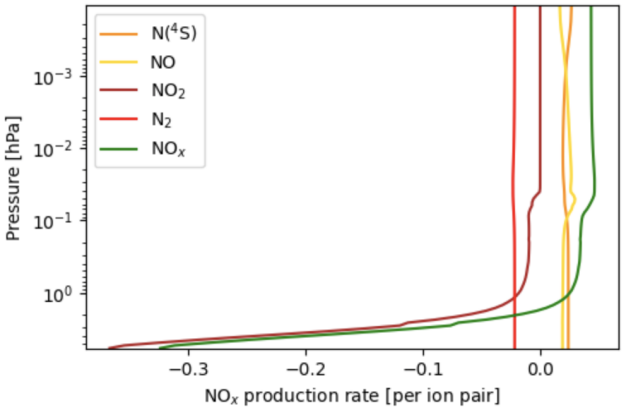

Figure 4.6: Mean production rates per ion pair of the NOx species (and N_2 for comparison).The sum of all NOx species shows a net production of NOx by the SPE until $\sim 2\times10^{0}$ hPa, at higher pressures NOx is even consumed.

$$NO_2 + OH \xrightarrow{M} HNO_3 \tag{4.4}$$

The contour plots of NO_3, HNO_3 and N_2O_5 can be viewed in the appendix in figure 7.4. In general, the NOx chemistry implemented in the model is very complex, as all these species are in a dynamical equilibrium with each other. This equilibrium is shifted through the production of N and NO during the event, similar to what is observed for HOx. The production rates, displayed in figure 4.6, show that NO_2 is not so much produced by the ion chemistry directly (instead it is even consumed at pressures higher than 5×10^{-2} hPa), but N and NO are produced in all layers. This results in a secondary production of NO_2 through neutral reactions (similar to HO_2), which is then effectively transferred to the NOx sinks as explained above.

4.3.2 Impacts on the catalytic cycles and the balance of CO_2, CO and O_2

4.3.2.1 Changes in CO_2, CO and O_2

The contour plots displaying the temporal evolution of the differences between event- and reference simulation for CO_2, CO and O_2 are shown in figure 4.7. As CO_2 is the major constituent of the atmosphere, its change is below 0.001% around 1×10^{-1} hPa, while

the changes of CO, O_2 and O are in the range of $< 0.2\%$, $< 0.05\%$ and 30%, respectively. As has been mentioned before, the most significant changes are visible in the range

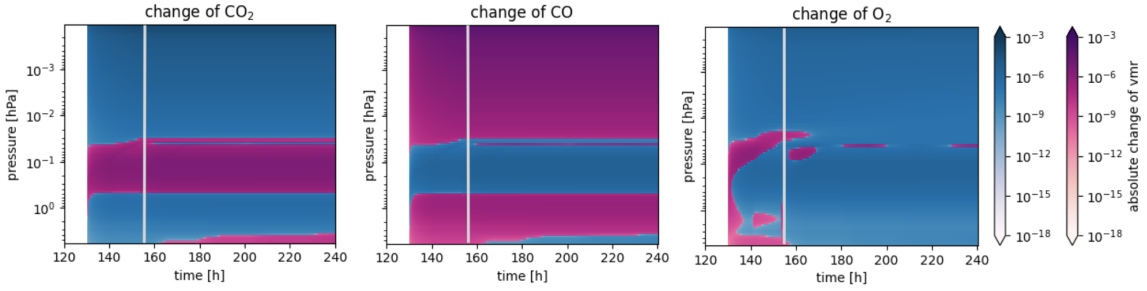

Figure 4.7: Temporal evolution of the differences of CO_2, CO and O_2 (day event simulation compared to the reference). The end of the event is marked with a light grey line.

of 5×10^{-1}-5×10^{-2} hPa, where a surplus of CO_2 is being created during the event. As can be seen when looking at the percentage changes, the anti-correlated change in CO clearly has a greater impact on its total abundance than it is the case for CO_2; that was to be expected since the volume mixing ratio is several orders of magnitude smaller. The CO_2 production is not caused by the event directly as can be seen in the production rates resulting from the ion chemistry, shown in figure 4.8: the charged particles cause a destruction of CO_2 (production of CO) in all atmospheric layers. Therefore, the observable surplus must result from indirect effects of the event on the neutral chemistry; a first hypothesis would suggest an enhancement of the efficiency of at least one of the catalytic cycles presented in section 2.2.3, which would result in a faster production of CO_2 relative to its destruction by photolysis, and therefore an increased abundance compared to the reference atmosphere.

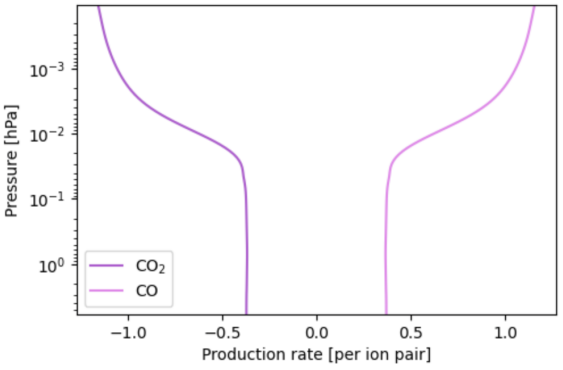

Figure 4.8: Mean production rates per ion pair of CO_2 and CO.

The formation of excess CO_2 is continued for 5-10 hours after the event, which correlates to the remaining daytime of day 7. The growth stops around the simulation hours 160-165 and the surplus remains stable for another 40 hours, before the degradation starts to predominate around hour 208, which corresponds to sunrise of day 9. From that point on, the surplus slowly starts do decrease until sunset, where it remains constant again until the end of the night. The correlating temporal evolution of CO_2 and CO can be seen in figure 4.9. This behaviour serves as the first indicator for a correlation between the CO_2 stability and the diurnal cycle. For the degradation this is expected, as the photolysis of

CO_2 is the only mechanism for that and is deactivated at night. For the production this could already indicate a predominant role of the photolysis-dependant cycles 2 and 3a, but this will by analysed in more detail in the following sections.

The assumption of dependency on daylight is further supported by the behaviour of CO_2/CO in the night start run: there, the event ends at night and with it the production of the CO_2 surplus. The amount reached remains constant over the course of the night until sunrise of day 7, from which on the CO_2 production is continued. The corresponding plots of the temporal changes are shown in figure 7.6 in the appendix.

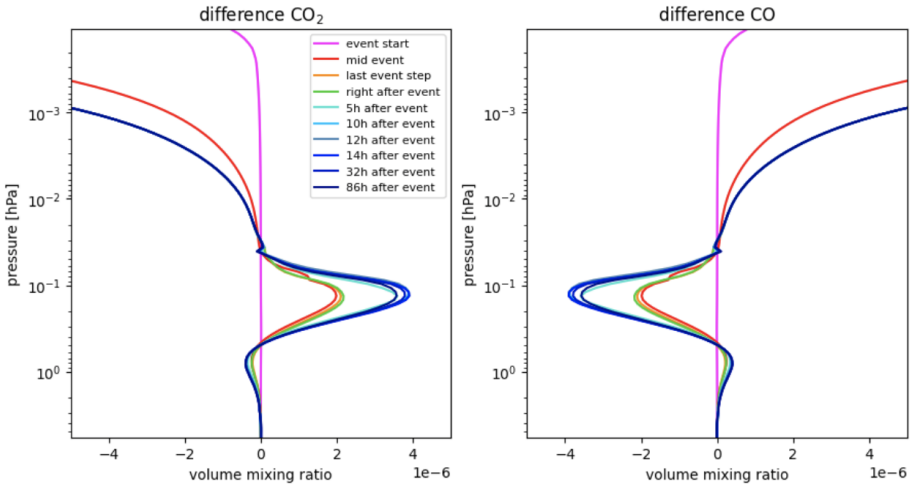

Figure 4.9: Temporal development of the changes of CO_2 and CO compared to the reference.

Comparison to O_2 and O

The comparison to the behaviour of O_2 and O regarding the orders of magnitude of the change and the temporal development might serve as a first indicator which net reaction of the catalytic cycles could play a dominating role in the CO_2 formation. In general, the net reaction 2 CO + O_2 → 2 CO_2 would expect a ratio of $\Delta CO : \Delta O_2 = 2{:}1$, while the net reaction CO + O → CO_2 would expect a ratio of $\Delta CO : \Delta O = 1{:}1$. However, as O is significantly more reactive than O_2, its observed changes might not exclusively be caused by this net reaction, therefore the comparison needs to be handled with caution.

The contour plot of O_2 (figure 4.7) shows that it is produced at a slightly higher altitude than the analysed pressure range, otherwise it is consumed. This does not fit the net production rates resulting from the SPE, therefore most of the changes must come form indirect impacts on the neutral chemistry. The temporal changes in the pressure range $7{\times}10^{-2}$-$5{\times}10^{-1}$ hPa, displayed in figure 4.10, fit to the changes in CO_2 and CO in form of the stoichiometry of the net reaction 2 CO + O_2 → 2 CO_2, which is especially visible in the long-term behaviour. Changes in O are only significantly observed at slightly lower pressures (higher altitudes) and are therefore not fitting the major changes of CO_2. What could be related is a change that is only visible in the red line representing the change dur-

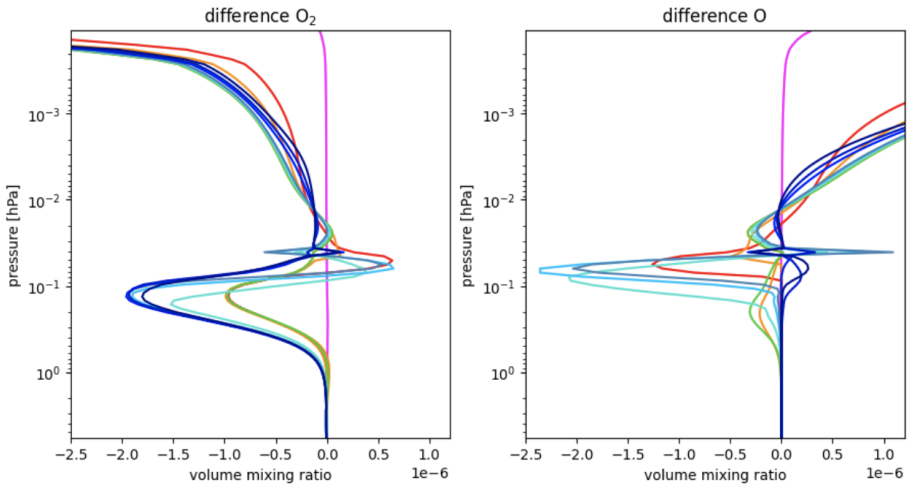

Figure 4.10: Temporal development of the changes of O_2 and O compared to the reference.

ing the event: there is a small bump visible in CO_2 and CO at around $8{\times}10^{-2}$ hPa, which could correlate to the peak in O (figure 4.10), as the stoichiometry fits the net reaction CO + O → CO_2. A more detailed comparison is shown in the appendix in figure 7.5.

Hypothesis

The correspondence of the changes in CO_2/CO and O_2 already imply a dominating role of the net reaction 2 CO + O_2 → CO_2, which would suggest an enhancement of (especially) the cycles 2 and 3a. This is further supported by the clear dependence on the diurnal cycle which is not only caused by the photolysis of CO_2 but also its production, as that is enhanced only during daytime after the event and would match the photolysis-dependence of the two cycles.

4.3.2.2 Changes in the catalytic cycles

HOx cycle 1 (see page 14)

To determine the rate-limiting step of the cycle, especially in the pressure range of interest, a comparison of all reaction rates has been done for both day and night which is shown in figure 4.11. The numbering of the reactions follows section 2.2.3.1. The v_i during daytime were taken from simulation hour 180, during nighttime from hour 170. As the changes in the rates due to the event are several orders of magnitude smaller than the absolute rate values, the order of the reaction rates is identical before/during/after the event. Therefore, the rate-determining step remains the same throughout the whole simulation.

As can be seen in figure 4.11, reaction 2 is the rate-limiting step at night, while during day all reactions have approximately the same rate (in the observed pressure range $5{\times}10^{-1}$-$5{\times}10^{-2}$ hPa). During daytime, v_1 behaves almost identical to v_2 and at night similar to v_3 at pressures higher than $2{\times}10^{-2}$ hPa, which is why the graph of v_1 is barely visible in

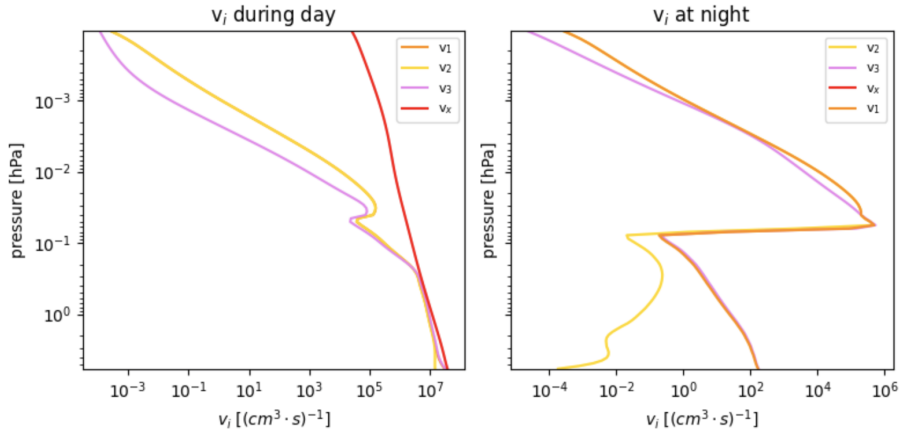

Figure 4.11: Comparison of the reaction rates of all steps in HOx cycle 1, including the photolysis of CO_2 (v_x).

both diagrams. Furthermore it can be seen that during daytime, the photolysis of CO_2 is faster than all reactions of the cycle, while at night it is deactivated.

Based on this, it can be assumed that a change in v_2 is decisive for a change in the rate of the net reaction. Therefore an analysis of the behaviour of v_2 compared to the reference calculation is done in the following. The contour plot which shows the temporal evolution of the change of v_2 is given in figure 4.12. The changes correspond to the behaviour of O and HO_2 which is expected, as a variation in the rate depends on a change in the concentrations of the reactants. As can be seen, the step is accelerated during the event from 4×10^{-1} hPa upwards during daytime, and in all layers at night. After the event, the reaction remains accelerated at night for the whole simulation while during the day, it starts to get decelerated completely from the sunrise of day 9 on (after hour 200). This behaviour corresponds to the observed behaviour of CO_2; the destruction of the accumulated surplus sets in from this time on. This can be explained as follows: while the production starts to get decelerated, the destruction through photolysis is still enhanced (due to the higher abundance of CO_2); therefore, the equilibrium between both processes shifts so that the destruction is more effective, resulting in a net consumption of the surplus. Before that, production and destruction have been in a (new) dynamical equilibrium, hence the stability of the accumulated excess over 40 hours. Although it should not be of relevance, it can be noted that the rate of the other two reactions, v_1 and v_3, show a similar behaviour as v_2, which is little surprising as the

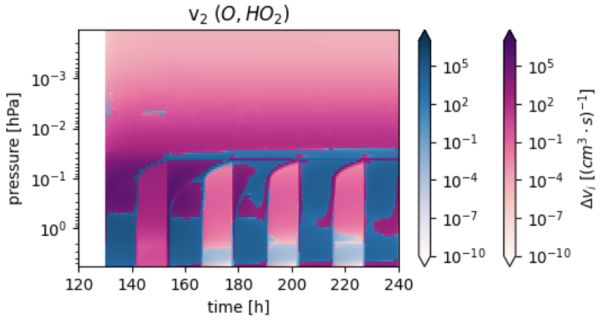

Figure 4.12: Change in the rate of reaction 2 in comparison to the reference atmosphere. Pink describes an acceleration, blue a deceleration.

reactands H and OH show a similar response to the event as HO_2 does.

HOx cycle 2 (see page 14)

The comparison of the reaction rates during day and night are shown in figure 4.13, analogous to cycle 1. As this cycle contains a photolytic reaction, this limits the effectiveness of the cycle at night, causing it to be inefficient during that time. At day, v_4 undercuts the photolysis, causing a switch regarding the rate-limiting step. Therefore, the temporal development of the change of v_4 is shown in figure 4.14.

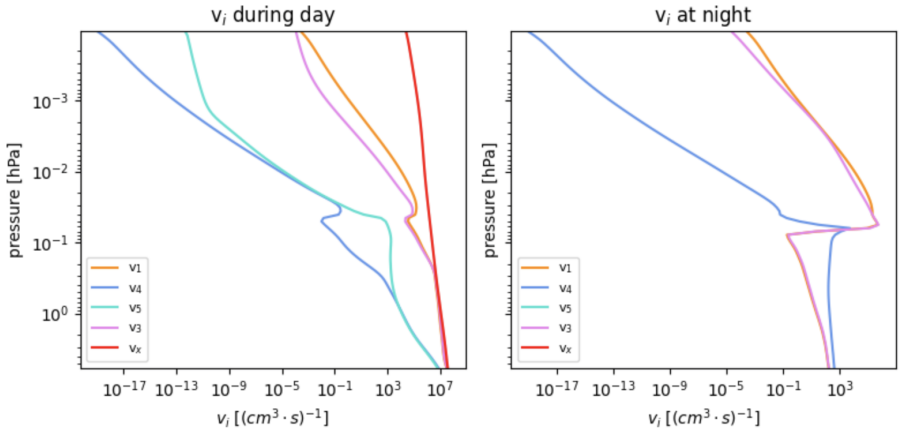

Figure 4.13: Comparison of the reaction rates of all steps in HOx cycle 2, including the photolysis of CO_2 (v_x).

As expected, the behaviour of v_4 is strongly correlated to the change of HO_2, as it is the self-reaction. Therefore, the reaction is accelerated during the event in all layers which continues afterwards until it starts to get decelerated compared to the reference during daytime after hour 186 (which corresponds to noon of day 8). During nighttime, the reaction is always enhanced, just as HO_2 is. With sunrise of day 9 (hour 200) the first day starts where the reaction is completely decelerated from sunrise to sunset. As photolysis is inactive at night, it is expected that the cycle is more or less turned off without solar irradiation.

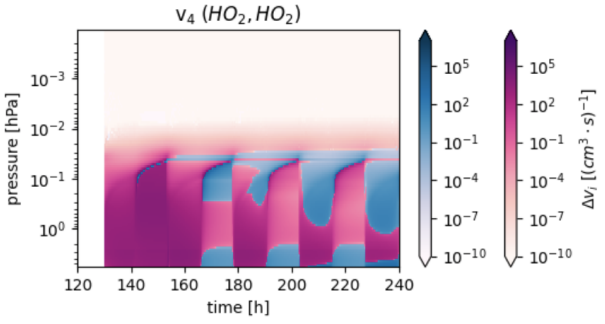

Figure 4.14: Change in the rate of reaction 4 in comparison to the reference atmosphere. Pink describes an acceleration, blue a deceleration.

These observations further support the explanation given for HOx cycle 1; therefore, the HOx cycles seem to be at least responsible for keeping the surplus stable during day until sunrise after hour 200; with the deceleration of the rate-limiting steps after that, the CO_2 photolysis overcomes the production, resulting in the observed net loss of CO_2. As

the behaviour of CO_2 seems to be dependant on the diurnal cycle, it could be assumed that this cycle might be more relevant than cycle 1. Otherwise, a continuous production of excess CO_2 during night times would be expected, as there is no competitive reaction active at night, while cycle 1 should be active at all times. Cycle 2 on the other hand fits the observation of a constant surplus during night times, as then simply both production and destruction are "turned off", resulting in no net change. This preliminary assumption is further supported by the observed ratio of the abundance changes, which fit the net reaction of cycle 2 ($\Delta CO{:}\Delta O_2 = 2{:}1$).

HOx/NOx cycle 3a (see page 15)

Just as HOx cycle 2, this coupled cycle is dependent on a photolytic reaction (7), too, which is therefore expected to be the rate-limiting step at night, causing the cycle to be inefficient when lacking solar irradiation. During day, it is also the photolysis which limits the net rate of the cycle, as can be seen in the comparison of the reaction rates in figure 4.15.

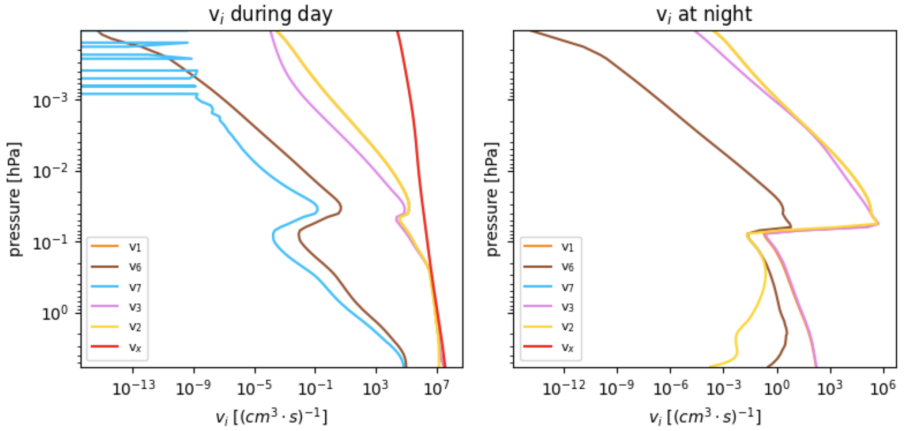

Figure 4.15: Comparison of the reaction rates of all steps in the HOx/NOx cycle 3a, including the photolysis of CO_2 (v_x).

The contour plot of the change of v_7 is shown in figure 4.16; the behaviour is clearly correlated to the change in NO_2 (which was expected). As previously seen in section 4.3.1.2, NO_2 is quickly being destructed after the end of the event around $1{\times}10^{-1}$ hPa and runs into a deficit. Same is therefore observed for v_7: its acceleration during the event is turned into deceleration over the course of day 7, 5-10 hours

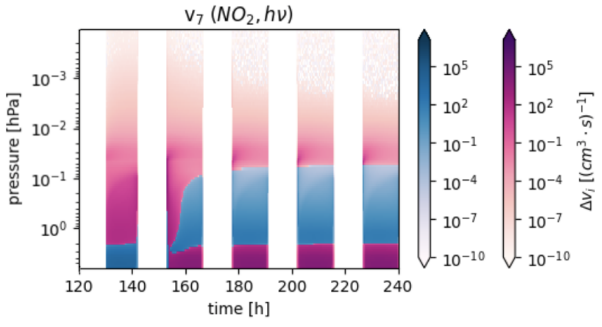

Figure 4.16: Change in the rate of reaction 7 in comparison to the reference atmosphere. Pink describes an acceleration, blue a deceleration.

after the event, which remains for the rest of the simulation. Therefore, the cycle is expected to be accelerated during and shortly after the event over the daytime of day 7 before it is decelerated. This behaviour could correlate with the formation stop of excess CO_2 around sunset of day 7, as the net reaction furthermore fits the observed abundance ratios as well as the inactivity at nighttime.

HOx/NOx cycle 3b (see page 15)

In contrast to cycle 3a, this coupled cycle is independent of photolysis, as the reaction is replaced by the reaction of NO_2 with O. Furthermore this cycle results in a net reaction similar to HOx cycle 1 which causes a consumption of O instead of O_2. The rate-limiting step at night is reaction 8, while during day the rates v_8 and v_6 are approximately the same around $1{\times}10^{-1}$ hPa, as can be seen in figure 4.17. The contour plots of both reactions

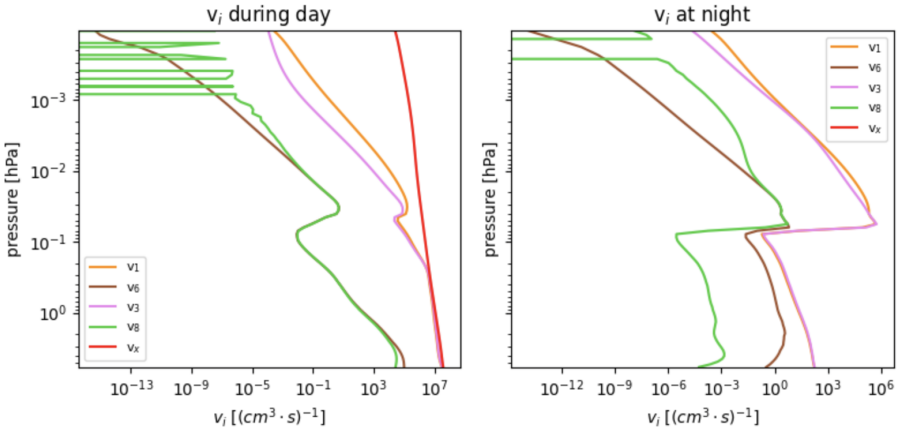

Figure 4.17: Comparison of the reaction rates of all steps in the HOx/NOx cycle 3b, including the photolysis of CO_2 (v_x).

are shown in figure 4.18; as can be seen, v_8 shows a similar behaviour during daytime as previously v_7 in cycle 3a. The switch from acceleration to deceleration happens already over the course of day 7, afterwards the reaction remains decelerated at daytime. During night, it is accelerated again; this behaviour results from the interplay of the changes in NO_2 and O. V_6 behaves more or less identical to v_8: it is also decelerated at daytimes from the middle of day 7 on with a reoccurring acceleration every night.

All in all, the behaviour of cycle 3b is very similar to cycle 3a, despite being independent from the diurnal cycle and the net reaction. If this cycle would be considered as superior, a reoccurring production of CO_2 would be expected at night times, as there is no degradation taking place while the cycle is enhanced. Since this is not the case, it is assumed that this mechanism only plays a subordinate role during and after the event.

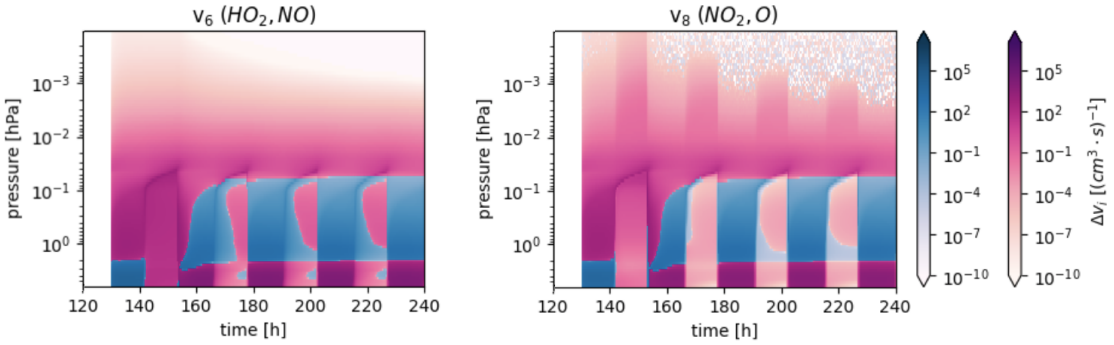

Figure 4.18: Changes in the rates of reaction 6 and 8 in comparison to the reference atmosphere. Pink describes an acceleration, blue a deceleration.

4.3.3 Conclusion and outlook

The changes in the abundances of CO_2, CO and O_2 that have been simulated during and after the event fit to the net reaction

$$2\ CO + O_2 \longrightarrow 2\ CO_2$$

as has been shown in section 4.3.2.1. Furthermore, the temporal evolution of the excess CO_2 shows a production during the event and during daytime afterwards, not at night. This is explicitly visible in the night run where the production only continues after sunrise on day seven, 10 hours after the end of the event instead of immediately afterwards. The respective diagrams are shown in the appendix in figure 7.6. After sunset of day 7, the surplus of CO_2 remains constant over several days (40 hours), independent of daytime, which indicates a dynamical equilibrium between photolytic decay and production during daytime, while both are being inactive at nighttime. After sunrise on day 9 (after hour 200), the excess starts to break down, indicating a shift in the equilibrium: the production is becoming slower while the photolysis is still at an enhanced rate.

All of this supports a CO_2 production that is dependent on photolysis in the same way as the destruction, as the respective catalytic cycles should be inactive at night, too, in order to explain the observed behaviour. A dominating role of the photolysis-independent cycles instead would lead to the expectation of an enhanced CO_2 production at night, as the competitive decay reaction is missing while the cycles are enhanced (according to the behaviour of the rate-limiting steps).

This leads to the final conclusion that cycles 2 and 3a are most likely to dominate the changes in the abundances of CO_2, CO and O_2, as they

1. drive the net reaction that fits the ratios of the changes
2. show a dependency on the diurnal cycle and cause therefore no CO_2 production at night
3. can together explain the temporal evolution of CO_2: Cycle 3a is responsible for the stop of further excess production at the end of day 7, as the rate-limiting step is being deceler-

ated shortly after the event due to the fast degradation of NO_2. The still accelerated cycle 2 counteracts the enhanced photolysis and stabilises the current CO_2 abundance (resulting in a new dynamical equilibrium with a higher CO_2 abundance compared to the reference period) until it is also decelerated during daytime from sunrise of day 8 on (after hour 200). This causes again a shift in the dynamical equilibrium, resulting in a slow degradation of the surplus in CO_2.

Nevertheless it has to be mentioned that the cycles 1 and 3b could play a supporting role at least during the event, which could explain the fitting abundances slightly above 1×10^{-1} hPa in the middle of the event as well as the continuous production during the event at night. The latter is especially visible in the changes of CO_2 during the event of the night run (contour plots are shown in the appendix in figure 7.7): the excess CO_2 is already starting to be produced in the first half of the event during nighttime, but only at pressures slightly lower than 1×10^{-1} hPa; this further supports a contribution of the cycles 1 and 3b at higher altitudes.

Outlook

It could be expected that over a longer time period after the event, the excess CO_2 is completely being degraded, while the other species (especially HOx and NOx) recover from their deficit so that the same conditions as in the reference atmosphere are met again. Due to the atmospheric drift of the abundances that is observed over the course of the simulation, it is unlikely that the initial conditions before the start of the event are reached again, but at least a decrease of the difference between event simulation and reference towards zero could be expected.

In order to further investigate this, simulations over a longer time period need to be done. As this correlates with increasing computation costs and duration, it could be considered to limit the event simulation explicitly to the pressure range that has been investigated in this chapter, which is 5×10^{-1}-5×10^{-2} hPa.

5. Venus

5.1 Simulation setup

The total simulation time was 240 hours as for Mars, although it corresponds to only 1/10 of a venusian day. Therefore, the whole simulation could have been run either at night or during day; as photochemical processes play a key role in this thesis, the final simulations were made during day, at a solar zenith angle of 80-70°. This interval has been chosen through a series of reference runs at different angles to evaluate the changes in photolysis intensity and to obtain mean abundance values of important atmospheric components, which is further explained in section 5.3. Other than for Mars, the simulation of Venus was restricted to the upper atmosphere: the lower boundary was chosen to be the cloud tops in approximately 70 km altitude, the upper boundary was fixed by the input file at 117 km. The resulting pressure range is very similar to Mars complete atmosphere, extending from 2.9×10^{1} hPa at the cloud deck to 1.5×10^{-4} hPa in 117 km. There were several reasons for the decision to restrict the altitude range:

1. The model appeared to have problems with the high pressures in the lower venusian atmosphere, resulting in numerical problems caused by relatively high reaction rates at high pressures. These problems could not be solved within the frame of the thesis work.
2. Due to the high opacity of the cloud layer, there is little data available for the middle and lower atmosphere, making a validation of the modeled abundances difficult. In addition to that a lot of open questions exist regarding the atmospheric chemistry in and below the cloud layer, which is believed to be mainly driven by thermal reactions instead of by photolytic processes [12](as little light is reaching the lower altitudes while the atmosphere is effectively heated up by the strong greenhouse effect).
3. Due to the high density of the cloud deck and the lower atmosphere, it is questionable whether precipitating particles even reach altitudes below the clouds or if the main effect is caused by subsequent downward transport of the species produced in upper layers. As the model does not include any type of transport, these secondary effects cannot be analysed anyways.

As the main cloud layer is ending below the defined lower boundary of the simulation,

heterogeneous chemistry was neglected as on Mars. All species considered here are therefore existing explicitly in the gaseous phase.
The location was set to 60° longitude and latitude, resulting in a solar zenith angle of 80-70°, which corresponds to a lower standing Sun. The reason for this was the apparent overestimation of photolysis of several components (especially CO_2 and H_2O as will be seen in section 5.3), which got slightly better with increasing angle. Starting point of the simulation was vernal equinox instead of perihelion, which should further decrease the intensity of the solar irradiation. Besides that, a second reference calculation during night time was made for which the location has been set to 120° longitude (resulting in a solar zenith angle of 110-100°). This was done to compare both day- and nighttime abundances to the available measurements, which were either mean abundances, measured at the terminator or on the night side only.

5.2 Implementation of sulfur- and expansion of chlorine chemistry

As ExoTIC did not include any sulfur chemistry and was missing chlorine reactions relevant for the SOx/ClOx cycle, the neutral chemistry was extended accordingly to enable a simulation of the catalytic cycles on Venus as complete as possible. The list of reactions was oriented on the cycles discussed in [12] and additional reactions were taken from other Venus models [21], [40] in order to further improve the simulation of the quiet atmosphere after the first implementations. Besides the photolytic dissociation of SO_2 and SO, which has been mentioned in [12], the photolysis of SO_3 and H_2SO_4 were added as well for completeness. If available, the respective rate constants k were taken from the JPL catalogue of 2019 [34]; otherwise original literature was used or the values were taken from the other models [40], [21]. A list of all implemented reactions is given in the tables 5.1 and 5.2, together with the respective literature used.

5.3 Simulating the quiet atmosphere

The height-resolved measurements that are currently available for the venusian atmosphere (listed in table 2.3) are compared to the abundances obtained after the 240 hours of simulation time for day and night, displayed in the appendix in figure 7.8 if not explicitly shown here. There, the yellow graph shows the simulated abundances during daytime with a solar zenith angle moving from 80 to 70°, the dark blue graph displays the abundances at night with a solar zenith angle moving from 110 to 100°. As for Mars, the abundances that were provided by the input file are also added to the diagrams. Here, their primary function is picturing the drift of the atmospheric composition, but they furthermore support the hypothesis of an over-prediction in photolysis as will be shown in the following paragraphs. The structure of continuous height profiles (if available) is implied with discrete

Table 5.1: List of the implemented neutral reactions.

reaction	**rate constant k[1]**	**literature**
$SO + O \xrightarrow{M} SO_2$	$1.3 \times 10^{-30} \times \left(\frac{T}{300}\right)^{-2.2}$	[40]
$SO + SO \longrightarrow SO_2 + S$	8.3×10^{-15}	[27]
$S + O_2 \longrightarrow SO + O$	$1.6 \times 10^{-12} \times e^{100/T}$	[34]
$ClO + SO \longrightarrow Cl + SO_2$	2.8×10^{-11}	[34]
$Cl + CO \xrightarrow{M} ClCO$	$3.2 \times 1.3 \times 10^{-33} \times \left(\frac{T}{300}\right)^{-3.8}$	[34], [21]
$ClCO + O_2 \xrightarrow{M} ClCO_3$	$(5.7 \times 10^{-15} \times e^{500/T})/$ $(1 \times 10^{17} + 0.05 \times M)$	[27]
$ClCO_3 + Cl \longrightarrow ClO + Cl + CO_2$	1×10^{-11}	[27]
$ClCO_3 + O \longrightarrow Cl + CO_2 + O_2$	1×10^{-11}	[27]
$SO_2 + O \xrightarrow{M} SO_3$	k_0^{298}=1.8×10^{-33} n= -2 k_∞^{298}=4.1×10^{-14} m= -1.8	[34]
$SO_3 + H_2O \xrightarrow{H2O} H_2SO_4$	$8.5 \times 10^{-41} \times e^{6540/T} \times [H_2O]$	[34]
$SO + O_2 \longrightarrow SO_2 + O$	$1.6 \times 10^{-13} \times e^{-2280/T}$	[34]
$SO + OH \longrightarrow SO_2 + H$	$2.6 \times 10^{-11} \times e^{330/T}$	[34]
$HCl + H \longrightarrow Cl + H_2$	$1.8 \times 10^{-11} \times e^{-1761/T}$	[41]
$Cl_2 + O \longrightarrow ClO + Cl$	$7.4 \times 10^{-12} \times e^{-1670/T}$	[21]

[1] Units of the rate constants: $[cm^3 \times (molecule \times s)^{-1}]$ for second order, $[cm^6 \times (molecule^2 \times s)^{-1}]$ for third order

Table 5.2: List of the implemented photolysis reactions.

photolysis reaction	**wavelengths [nm]**	**literature**
$SO_2 \xrightarrow{h\nu} SO + O$	180-395	[42], [43], [44], [45]
$SO \xrightarrow{h\nu} S + O$	191-234	[46]
$SO_3 \xrightarrow{h\nu} SO_2 + O$	180-330	[34]
$H_2SO_4 \xrightarrow{h\nu} SO_3 + H_2O$	121.5, 195-330, single bands in 515-745	[47], [48]

measurement points to show its course. For species of which only rough abundance-ranges are available, the respective intervals are marked with rectangles. The colours of the measurements explain their origin: green indicates ground-based measurements, turquoise spacecraft-based measurements, pink model data obtained by Stolzenbach et al. with their PCM model [21]. A short description of the comparison of simulation and measurements is given in the following.

Similar to Mars, the abundance of CO_2 in the upper part of the simulation (which refers to a similar pressure range) is under-predicted, while CO is overpredicted as can be seen

in figure 5.1. As the comparison of the abundances of CO_2 and CO during night with the measurements show a very good agreement, it can be assumed that the reason is again a too strong photolysis. This is further supported by the fact that the nighttime simulation remains almost identical to the initial abundances, while the daytime simulation drifts away significantly.

N_2 is corresponding to the mean abundance, as it is not significantly influenced by the neutral chemistry (due to high energy that is needed to break the N-N bond) and therefore remains close to the input values. O_2 again is being over-predicted, whereas the abundances at night fit the averaged values of the PCM model from Stolzenbach et al. [21], as shown in figure 5.1. The over-prediction of O_2 is a common problem in all published Venus models and is up to now unsolved. [30] The simulated abundance of O_3 on the other hand is in fairly good agreement with the available measurements, even though they have been made on the night side only.

Although the ground- and spacecraft-based measurements of HCl stand in conflict with each other, the model ends up between the measured abundances and is therefore agreeing with both to the same degree.

The dayside-predictions of ClO are significantly under-predicted compared to the ground-based measurements, while the nightside simulation is from 80 km upwards in very good agreement with the PCM model [21]. At lower altitudes ClO rushes into very low abundances, which is most likely in strong disagreement with the reality, but there is no data available for actual comparison.

The day- and night simulations of H_2O frame the mean abundance-range that has been measured for above the cloud layer, therefore it is overall assumed as tolerable. Here again it could be argued that the photolysis of the model might be slightly too strong, resulting in an under-prediction of H_2O at daytimes, which ends up being not too big as H_2O is over-predicted at night, caused by the too high abundances provided by the input file. The comparison is displayed in figure 5.1.

Both SO_2 and SO are in very good agreement with the measurements done at the terminator, especially since the daytime simulations were made with a low-standing Sun. One negative aspect is nevertheless the disappearance of SO only around 100 km at night, but since the subsequent event simulations were done during daytime only, this aspect can be neglected. Comparing the simulations to the initial abundance of SO_2 it can be seen that the neutral sulfur chemistry seems to resolve the initially strong under-prediction.

H_2O_4 in turn experiences a similar problem as H_2O (under-prediction at day time) which is caused by the fact that the only formation path of H_2SO_4 is the reaction of H_2O and SO_3

$$SO_3 + H_2O \xrightarrow{H_2O} H_2SO_4$$

and the only destruction mechanism its photolysis. The nighttime simulations on the other hand are in very good agreement with both PCM model [21] and ground-based measurements (which determined an upper limit).

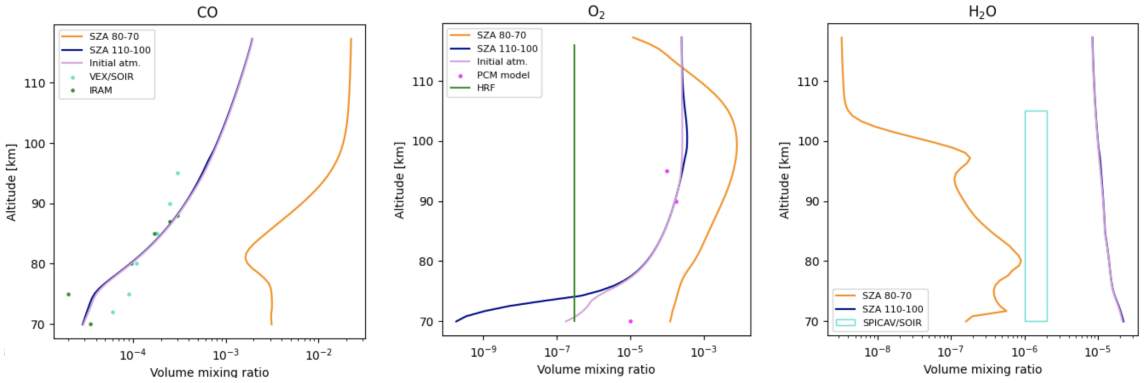

Figure 5.1: Comparison of simulation results and initial compositions with the available measurements for CO, O_2 and H_2O.

5.4 Simulation of the Solar Particle Event

As the diurnal cycle is playing no role in the defined simulation period, only one event simulation was made. The event start was set to 120 hours (like the first run of Mars), lasting 24 hours, ending after hour 144. The remaining 96 hours were used to analyse the response of the atmospheric chemistry to the disturbance, as previously explained for Mars.

5.4.1 Changes in NOx and HOx: Comparison to Earth and Mars

Similar to Mars, the most relevant changes are in the pressure range of 1×10^{0}-5×10^{-2} hPa, as there is the most significant change in the abundances of CO_2/CO/O_2 observable (this will be further discussed in section 5.4.2). This and the fact that changes in lower pressure ranges are more or less irreversible over the course of the simulation, are the reason why the upcoming analysis will focus on the defined pressure range.
Although the production rates of both HOx and NOx due to the direct impact of the charged particles are mostly very similar to the event on Mars, the behaviour of the species in the atmosphere afterwards is strikingly different. This could be attributed to the missing diurnal cycle in the venusian simulation, different abundances of other species and therefore a different dynamical equilibrium.

5.4.1.1 Changes in the HOx budget

In general, the behaviour of HOx is rather similar to that of NOx in the martian atmosphere (instead of HOx) despite the fact that the relative changes are significantly lower: For H

and OH it is in the range of 3%, for HO_2 in the range of 6%. The temporal evolution of the changes in the HOx species are displayed in figure 5.2. In comparison to the relative changes that have been observed on Earth (see section 2.1.2), the HOx production seems to be comparable to stratospheric OH but significantly lower than the values reached in the mesosphere. A simple explanation for this might be the low abundances of H_2O and H_2 in the venusian atmosphere.

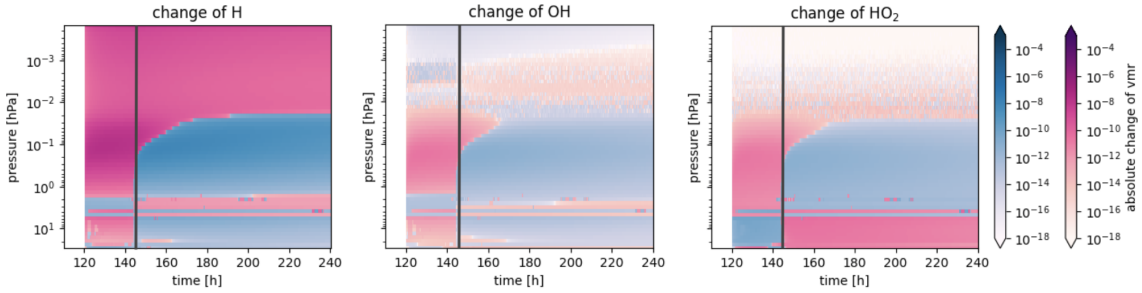

Figure 5.2: Contour plots of the changes in H, OH and HO_2 compared to the reference. Blue describes a deficit, pink a surplus in comparison to the quiet atmosphere. The end of the event is marked with a grey line.

Unlike on Mars, all HOx species on Venus show the same behaviour which is why they do not need to be described separately: During the event, a surplus of all HOx species is being produced, strongest around $1{\times}10^{-1}$ hPa. The production fits the production rates caused by the SPE which are shown in figure 5.3. The accumulated surplus is broken down immediately after the event and switches into a more or less strong deficit instantaneously,

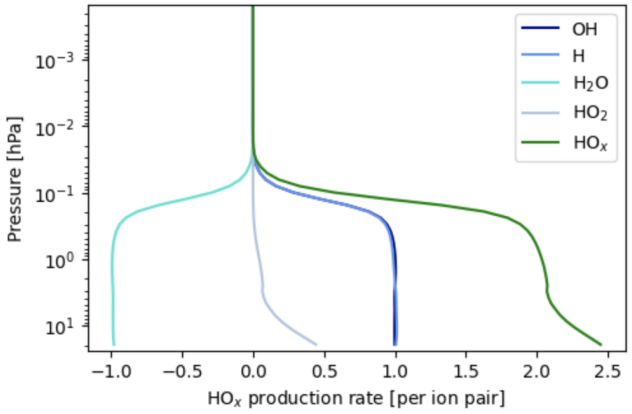

Figure 5.3: Mean production rates per ion pair of the HOx species (and H_2O). As the rates are plotted linear, the rates above $3{\times}10^{-2}$ hPa appear to be ∼0; this is not the case. The production of HOx due to the event is in all layers >0, just several orders of magnitude smaller above $3{\times}10^{-2}$ hPa.

which remains until the end of the simulation and recovers only slowly. The reason for that is similar to the explanation for Mars: Instead of a complete recovery of H_2O, part of it is transferred to H_2 as can be seen in the orders of magnitude and temporal evolution of the changes in both species, shown in figure 5.4. The oxygen of the remaining H_2O-deficit is most likely spread over different oxygen-bearing species that are found to be in a slight surplus at the end. What cannot be observed in analogy to the martian simulation is H_2O_2 serving as a temporal HOx reservoir, as the further transformation to H_2O and H_2 might be significantly faster than under martian conditions. This is probably caused by

the continuous and fast photolysis of H_2O_2, as on Venus the diurnal cycle plays no role over the course of the simulation. Furthermore, photolytic reactions are expected to be much stronger in general since Venus is significantly closer to the Sun and therefore exposed to more intense solar irradiation.

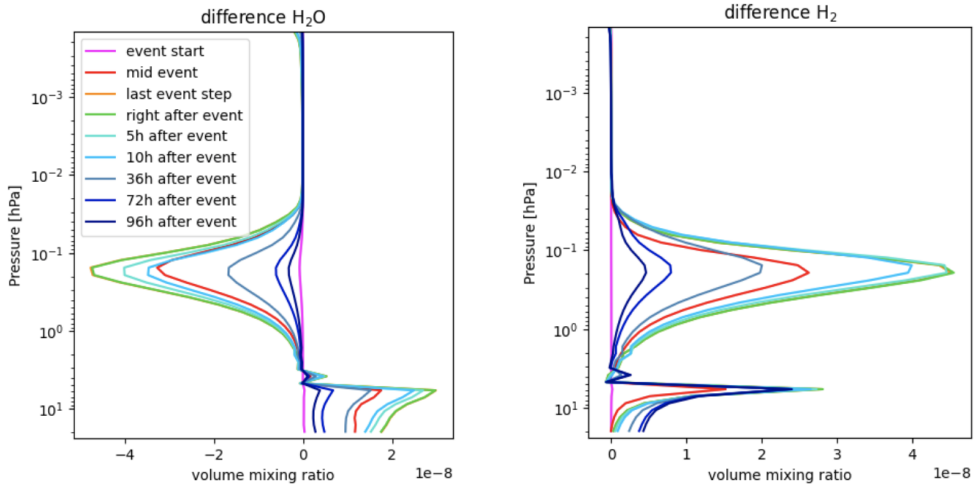

Figure 5.4: Temporal evolution of the differences of H_2O and H_2 (event simulation compared to reference).

5.4.1.2 Changes in the NOx budget

Apart from N, NOx on Venus shows a very different behaviour compared to Mars and is rather comparable to the polar regions on Earth, where excess NOx that is being produced due to a SEP seems to be more persistent than in other regions. During the event, the percentage increase of NOx is similar to the simulation for Mars in the range of $10^3 - 10^6$% and therefore again very high. The NOx production rates (figure 5.5) caused by the precipitating particles are positive in all layers, with exception of NO_2 at pressures higher than $2{\times}10^0$ hPa, where it is most likely produced through enhanced neutral formation reactions (due to increase in NO and N). The NOx surplus that is accumulating over the course of the event in all layers remains afterwards until the end of the simulation and is only slowly reduced, as can be seen in the temporal evolution of the changes in figure 5.6. The degradation of NO and NO_2 seems therefore to be significantly

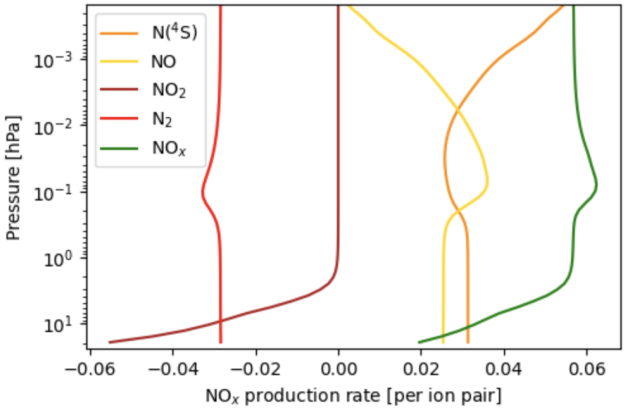

Figure 5.5: Mean production rates per ion pair of the NOx species (and N_2 for comparison).The sum of all NOx species shows a net production of NOx by the SPE in all layers, which is different to Mars.

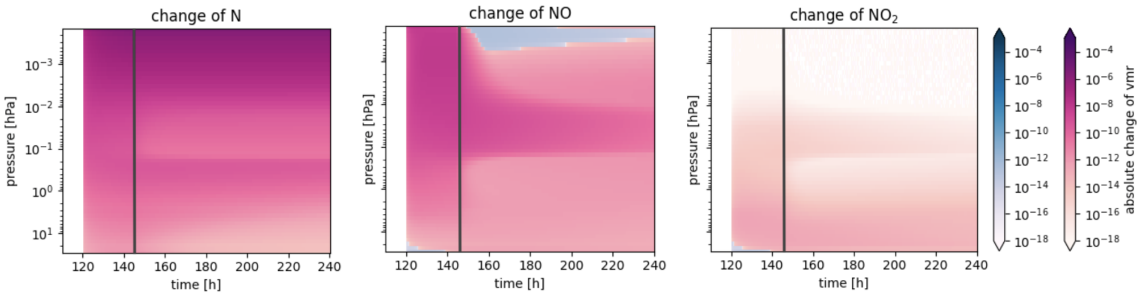

Figure 5.6: Contour plots of the changes in N, NO and NO_2 compared to the reference. Blue describes a deficit, pink a surplus in contrast to the quiet atmosphere. The end of the event is marked with a grey line.

slower than on Mars, as it further does not run into a deficit. In agreement to that, the NOx reservoirs NO_3, HNO_3 and N_2O_5 experience only minor increases, several orders of magnitude lower as on Mars. The respective contour plots are displayed in the appendix in figure 7.10. An explanation for this must be the missing diurnal cycle. As it has been shown for Mars, the reservoirs are preferably produced at night, when photolysis is inactive and the species are stable. As the photolytic processes are constantly active on Venus, a continuous re-emission of NO and NO_2 is happening, blocking the efficient capture of the excess NOx in stable reservoirs.

5.4.2 Impacts on the catalytic cycles and the balance of CO_2, CO and O_2

5.4.2.1 Changes in CO_2,CO, O_2 and O

Similar to Mars the pressure range of most relevance is $5{\times}10^{-2}$ to $1{\times}10^{0}$ hPa, reaching down to only slightly higher values. In these layers, a strong excess production of CO_2 is observed during the event, which, in contrast to Mars, is not continued afterwards. Instead, the production stops immediately after the end of the event and turns into degradation approximately 5 hours afterwards, resulting in a decrease of the CO_2 surplus. From day 9 on, this even turns into the development of a deficit compared to the reference atmosphere. The contour plots of the changes in CO_2 and CO are shown in figure 5.7. As CO_2 is again the major constituent of the atmosphere, its relative change is below $3 \times 10^{-4}\%$ in the analysed pressure range, which is around half the value obtained for the event on Mars. The change of CO is accordingly only in the range of $< 0.1\%$. Based on the observations described above, the destruction of the excess CO_2 seems to happen much faster than on Mars, resulting even in a switch into a deficit. One similarity in turn are the net production rates: the CO_2 production during the event cannot result from the ion chemistry directly, as this is causing a CO_2 destruction in all layers. Therefore, the change must be caused by the neutral chemistry, which is impacted by the changes of the other reactants due to the event, e.g., HOx and NOx. Analogous to Mars, this finding serves as a first indicator for an enhancement of the catalytic cycles during the event to explain the excess CO_2.

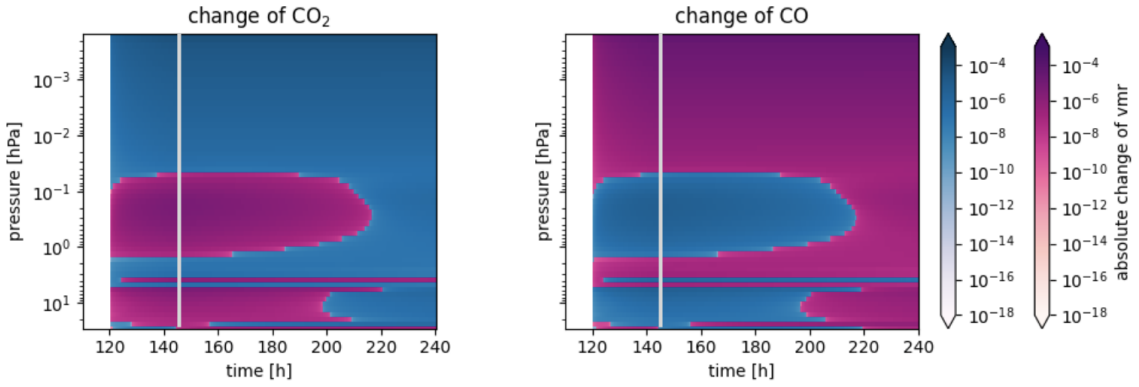

Figure 5.7: Temporal evolution of the differences of CO_2 and CO (event simulation compared to the reference). The end of the event is marked with a grey line.

Comparison to O_2 and O

The relative changes of O_2 and O are below 0.1% and 3.5%, respectively. The value for O_2 is therefore similar as on Mars, while O seems to experience a significantly lower relative change. But since O is a very reactive species, this value should not be given too much importance.

The general behaviour of O_2 fits the changes in CO_2 in the following aspects: the development of a deficit during the event is observed in the same pressure range (correlated to CO, anti-correlated to CO_2), which turns into a surplus at the beginning of day 9, according to the CO_2 deficit. Unlike on Mars the ratio of the changes in CO and O_2 do not fit perfectly to a certain net reaction, e.g., 2 CO + O_2 → CO_2. This is not surprising, as for Venus there are several net reactions assumed for the cycles, resulting in different ratios:

HOx 1	$CO + O \rightarrow CO_2$
HOx 2, HOx/NOx	$2\ CO + O_2 \rightarrow 2\ CO_2$
SOx/ClOx	$CO + O_2 \rightarrow CO_2 + O$
HOx/NOx/SOx	$CO + O_2\ (+\ SO_2 + H_2O) \rightarrow CO_2\ (+\ H_2SO_4)$

Therefore, there cannot be identified one certain net reaction to be responsible for the excess production, instead a group of several reactions might share the dominating role. Detailed plots of the temporal evolution of the differences of all four species with focus on the duration of the event are shown in figure 5.10. From there, it can be seen that the ratio of$\Delta CO:\Delta O_2$ is greater than 2:1 after the end of the event, meaning some CO does probably not consume O_2 for oxidation. The exact absolute values of the differences are 5.2×10^{-6} for CO and 2.3×10^{-6} for O_2, resulting in a ratio of 2.26:1. This is further supported by the different shape of the curves right after the event: The peak of CO is slightly broader, extending to higher altitudes (lower pressures). Furthermore interesting is the evolution of the differences shortly after the event: 5 hours afterwards, the differences of CO and O_2 do fit, as the deficit of O_2 continues to increase to 2.6×10^{-6} and broadens to higher altitudes,

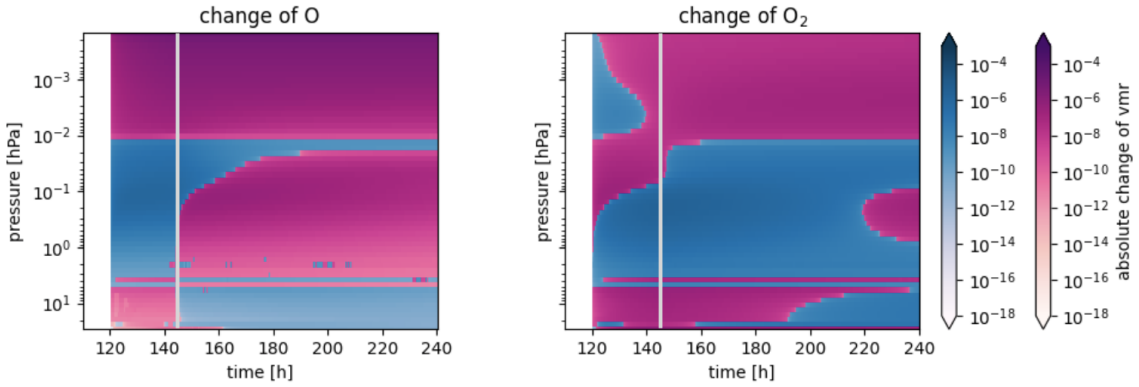

Figure 5.8: Temporal evolution of the changes in O_2 and O (event simulation compared to the reference). The end of the event is marked with a grey line.

resulting in a ratio of 2:1. It could be assumed that the balance between production and destruction of CO_2, which is established in the first 5 hours after the event as there is no net change in the accumulated surplus observed, is dominated by the net reaction

$$2\ CO + O_2 \rightarrow 2\ CO_2$$

while before that, several reactions were involved. But this cannot be said with certainty as the ratios of the changes do not enable a clear answer. What can be said is that the net reaction

$$CO + O_2 \rightarrow CO_2\ (+\ O)$$

did most likely not play a dominating role at any point of the simulation, as the ratio is far away from 1:1. To also take the direct impact of the event on to the Ox budget into consideration, a look is taken on the production rates (displayed in figure 5.9): At first, it could be assumed that the changes in O_2 result from the ion chemistry directly, as there is a peak similar to the deficit visible. But when taking a closer look, it can be seen that the deficit of O_2 appears at slightly lower levels (higher pressure). In addition to that it could be expected that the changes in O_2 (and also CO_2, CO) caused by the event directly are smaller than the changes due to the neutral chemistry, as the ratios of the differences observed in the Mars simulation (section 4.3.2.1) could be assigned very clearly to one net reaction and therefore a group of catalytic cycles. If the impacts would have been in the same orders of magnitude there, the behaviour most likely would have been different.

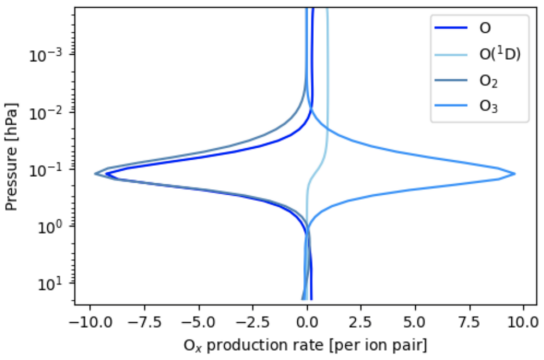

Figure 5.9: Mean production rates per ion pair of the Ox species.

Taking a look at the changes of O might enable a further specification of the involved net reactions: there, the development of a deficit can be seen during the event which recovers quickly afterwards. This happens at slightly higher altitudes (lower pressures) than the changes in O_2 and could therefore explain the broader line of CO_2; So could the excess CO_2 in lower levels be mainly produced with O_2, in higher levels with O. This does nevertheless not explain why the O_2 deficit moves to higher altitudes after the event.
Another striking feature that can be seen in the behaviour of O is that the deficit is reaching a maximum in the middle of the event and then decreases again. Its maximum value is -1.2×10^{-6}, while CO is at 2.7×10^{-6}, resulting in a ratio $>$ 2:1, supporting the assumption of the influence of several net reactions. It is also probable that the decrease of O during the first half of the event is caused by the ion chemistry directly, as the net production rate due to ionisation behaves exactly the same; yet the decrease of the deficit in the second half must be caused by the neutral chemistry, since the production rates by ion chemistry do not significantly change over the course of the event. Therefore, some reaction must produce O. One assumption could be the net reaction

$$CO + O_2 \rightarrow CO_2 + O$$

but this does not fit the pressure ranges, since the recovery of O happens at exactly 1×10^{-1} hPa, while the change in CO/CO_2 happens at 2×10^{-1} hPa. The fast recovery of O after the event, resulting even in a surplus, is explainable with the destruction of CO_2 through photolysis which produces O.

Hypothesis

The CO_2 production is being accelerated during the event, exceeding the degradation by photolysis. The latter is always active over the course of the simulation, as one diurnal cycle extends over a much bigger time period (which is an important difference compared to the Mars simulation). With the end of the event, the production stops and the accumulated surplus remains constant for a few hours, indicating that a new dynamical equilibrium between production and destruction is reached (and kept at least for a short time). Then the excess starts to be degraded, which speaks for a deceleration of the dominating catalytic cycles relative to CO_2 photolysis. The destruction causes a turn from surplus to deficit around the start of day 9, which indicates a shift in the dynamical equilibrium between production and destruction to a balance that is different compared to the reference atmosphere. This raises the expectation that the catalytic cycles are strongly decelerated at the end of the simulation time, starting that behaviour already after the end of the event. Unfortunately the changes in O_2 and O do not allow a clear hypothesis regarding the dominating catalytic cycle, as they all show too many different net reactions where

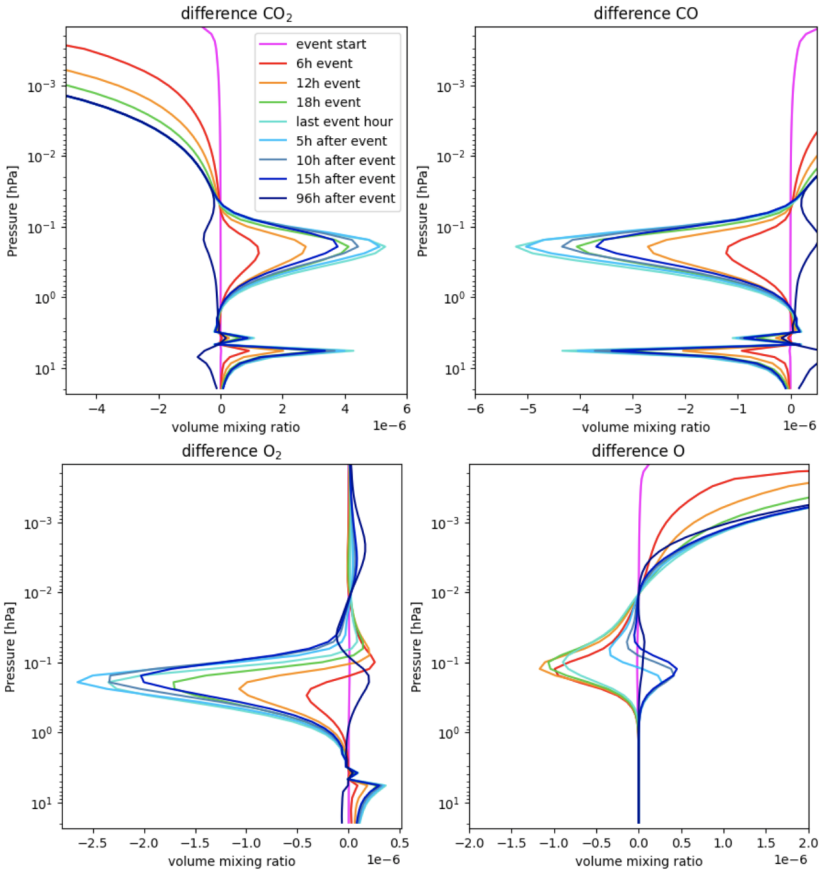

Figure 5.10: Temporal evolution of the differences of CO_2, CO, O_2 and O (event simulation compared to the reference) with focus on the event duration.

one is even producing O instead of consuming it. For now, it is assumed that the observed changes in CO_2/CO, O_2 and O are caused by a combined effect of several net reactions.

5.4.2.2 Changes in the catalytic cycles

HOx cycle 1 (see page 16)

The numbering of the reactions and rates here is according to the numbering done earlier in the presentation of the catalytic cycles in section 2.2.3. As can be seen in figure 5.11, the third reaction which is the CO_2-forming step appears to be the rate-limiting step of this cycle. As the changes in the rate caused by the disturbance do not have an effect on the reaction order (slowest to fastest), the v_i are shown only during the event. When looking at the changes of the rates compared to the reference atmosphere, it can be seen that all three reactions show a very similar

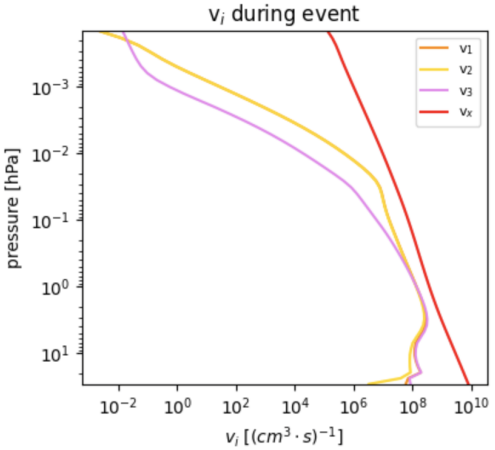

Figure 5.11: Comparison of the reaction rates of all steps in the HOx cycle 1, including the photolysis of CO_2 (v_x).

behaviour. This is caused by the changes in the abundances of the HOx species that are involved and were shown in section 5.4.1.1 to behave almost identical. The contour plot of the change of the rate of reaction 3 is displayed in figure 5.12. The first impression could suggest that this cycle might play an important role in the excess CO_2 production, because the rate-limiting step 3 fits the behaviour of CO_2: in the pressure range $5{\times}10^{-2}$ to $1{\times}10^{0}$ hPa it is strongly accelerated during the event, which switches into strong deceleration almost immediately afterwards and remains like that for the rest of the simulation. This could explain the degradation starting after the event end which causes the development of a deficit over the last two days. There cannot be made any further assumptions based on the net reaction of the cycle ($CO + O \rightarrow CO_2$), but due to the analysis that has been done in section 5.4.2.1, the cycle might rather be relevant during the first part of the event, before the start of the recovery of O.

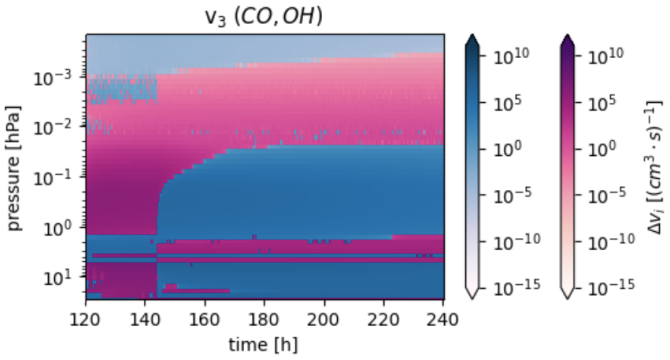

Figure 5.12: Change of the rate of reaction 3 in comparison to the reference atmosphere. Pink describes an acceleration, blue a deceleration.

HOx cycle 2 (see page 16)

The comparison of the reaction rates in figure 5.13 identifies reactions 4 and 5 to be both comparably slow, although reaction 5 might be slightly slower at the lower boundary ($1{\times}10^{0}$ hPa), which is the photolysis of H_2O_2. The rates are again compared only at one time step (here during the event), as the order of the rates does not change over the course of the simulation. Independent of which reaction is considered to be rate-determining, both show a similar behaviour which is in analogy to the other HOx reactions. Therefore, this cycle is expected to behave the same way as HOx cycle 1: strong acceleration during the event, which is in

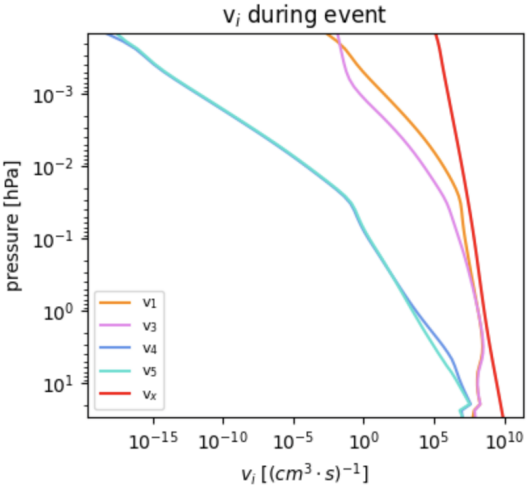

Figure 5.13: Comparison of the reaction rates of all steps in the HOx cycle 2, including the photolysis of CO_2 (v_x).

agreement with the observed CO_2 production, and then a deceleration afterwards until the end of the simulation, which could explain the occurring CO_2 destruction. The change of v_5 compared to the reference simulation is shown in figure 5.14. The only difference to the previous HOx cycle is the net reaction:

$$2\ CO + O_2 \rightarrow 2\ CO_2$$

Here, a consumption of O_2 is happening, which is at least not in conflict with the observed changes in O_2, although again no clear statement can be made in that context.

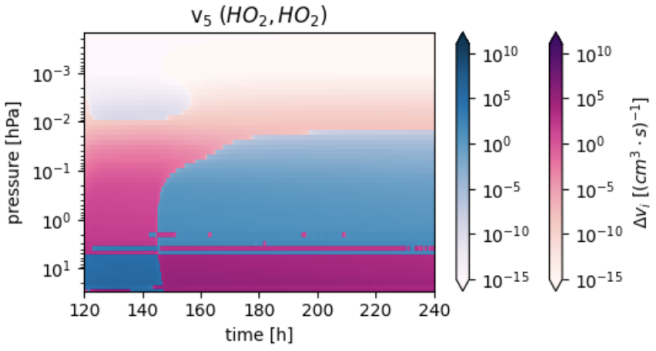

Figure 5.14: Change of the rate of reaction 5 in comparison to the reference atmosphere. Pink describes an acceleration, blue a deceleration.

SOx/ClOx cycle (see page 17)

In this cycle, the rate-limiting step is not a HOx reaction, but instead the chlorine-involving step that is responsible for the CO_2 production, as can be seen in the comparison of the v_i in figure 5.15. In contrast to the HOx reactions none of the reactions included in this cycle supports the observed behaviour of CO_2. The change of rate of reaction 9, that is found to be the rate-limiting step, is shown in figure 5.16. Looking at its behaviour in the pressure range of interest reveals that although it is partly accelerated during the event, this only happens at the boundaries. In the main part of the area a strong deceleration is observed instead which stands in conflict with the surplus production of CO_2. Afterwards, the reaction experiences a strong acceleration in the whole pressure range that remains until the end of the simulation, strengthening the disagreement

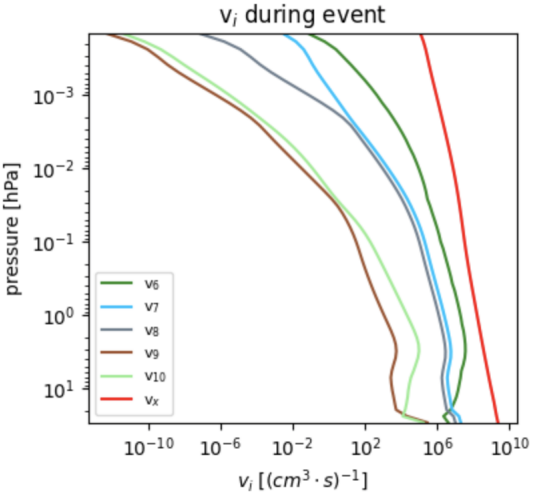

Figure 5.15: Comparison of the reaction rates of all steps in the SOx/ClOx cycle, including the photolysis of CO_2 (v_x).

with the changes in CO_2. An attempt to bring these contrary observations together could be the following hypothesis: the opposite behaviour of the SOx/ClOx cycle could have an inhibiting effect on to the HOx cycles, meaning the changes of CO_2 would be more extreme otherwise (a stronger surplus production during, and a faster degradation after the event). This would also mean that this cycle does not have the major impact on the changes in the CO_2 budget, which is a different outcome than expected, since especially the chlorine chemistry has been assumed to play the dominating role in the stability of CO_2 (see end of section 2.2.3.2).

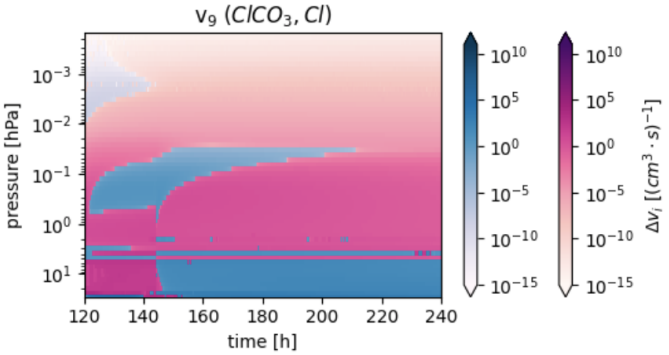

Figure 5.16: Change in the rate of reaction 9 in comparison to the reference atmosphere. Pink describes an acceleration, blue a deceleration.

HOx/NOx cycle (see page 17)

Similar to the first coupled HOx/NOx cycle on Mars the rate-limiting step here is the photolysis of NO_2 (reaction 12), as can be seen in the comparison in figure 5.17. As the changes of NOx are in the range of several thousand percent, the changes of the rates are visible even in the absolute values (not just in the decimal places, e.g., as in the HOx reactions). Therefore, the v_i are compared during and after the event. The noise in v_{12} at high altitudes is caused by the very low abundances of NO_2 there after the event. When its value falls below a lower boundary that has been set in the code, it is set to zero, which causes the reaction rate to become zero, too. Looking at the rate changes due to the disturbance, it stands out that the reaction is not only being accelerated during the event, but that it remains this way until the end of the simulation. This behaviour is little surprising as it has been shown earlier in section 5.4.1.2 that the destruction of the surplus in NO_2, that is produced during the event, happens only very slowly, remaining in a surplus over rest of the simulation. The temporal change of v_{12} can be seen in figure 5.18. Therefore it can be assumed that the net reaction of this cycle shows a similar behaviour and is enhanced accordingly. In comparison with the behaviour of CO_2, this could only support the excess production during the event, while the sustained acceleration afterwards expects a contrary course than is observed. This brings up a similar hypothesis as for the previous cycle: the acceleration after the event could have caused a damping of the CO_2

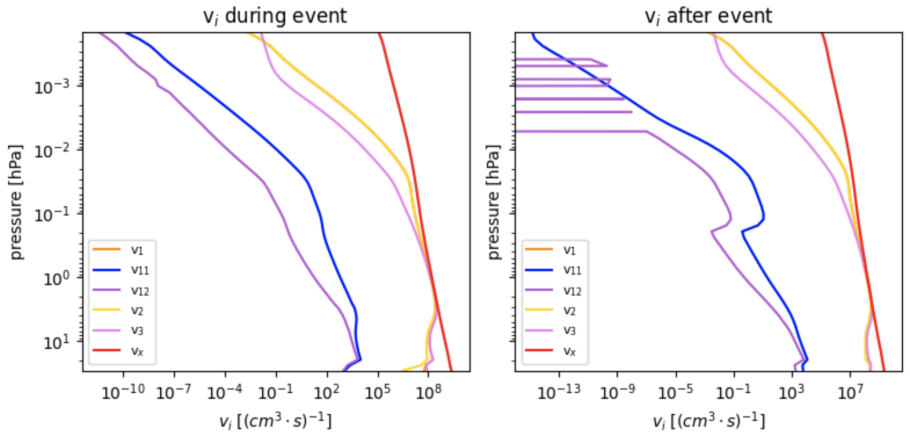

Figure 5.17: Comparison of the reaction rates of all steps in the HOx/NOx cycle during and after the event, including the photolysis of CO_2 (v_x).

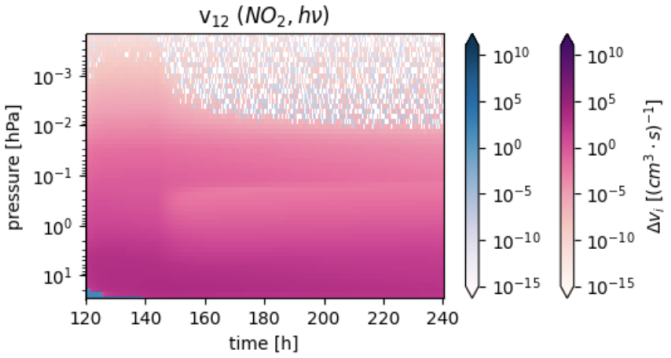

Figure 5.18: Change of the rate of reaction 12 in comparison to the reference atmosphere. Pink describes an acceleration, blue a deceleration.

degradation that is caused by the HOx cycles. The net reaction of the cycle supports the ratio CO:O_2 = 2:1, which is at least observed to a certain degree during the event.

An alternative hypothesis, based on the complexity of the cycles, possible external reaction paths and other non-linear effects, could be that not one of the NOx-dependent reactions is limiting the cycle, but instead one of the HOx reactions that are involved, too. This would lead to a behaviour fitting the temporal evolution of the CO_2 surplus.
As mentioned in section 2.2.3.3 it is hard for complex mechanisms to simply determine the rate-limting step based on one parameter, as there are a lot of factors that need to be considered. For isolated mechanisms that are assumed to be in steady state, the comparison of the rate constants k_i is decisive, but here this cannot be done alone. Yet, it might be an option in order to consider alternative hypotheses, which is why it has been done for this HOx/NOx cycle. The comparison of the k_i is shown in figure 5.19. Since only reaction rates with the same unit are comparable, the photolysis rates are not included here (they are of first order, while all others are of (effective) second order). It can be seen that instead

of reaction 12, reaction 1 is assumed here to be the rate-limiting step, which involves H as a reactant. As the changes of all HOx reactions fit the observed behaviour of CO_2, the net change of this HOx/NOx cycle would fit that way, too.

The assumption of the rate constants being decisive about the rate limiting step instead of the reaction rates does not change the interpretation of the SOx/ClOx cycle although the rate-determining step switches from 9 to 7, as both reactions show the same behaviour in the analysed pressure range. Same applies to the HOx cycles, since there all reaction steps support the observed behaviour of CO_2. The comparisons of the k_i for all three cycles are displayed in the appendix in figure 7.11.

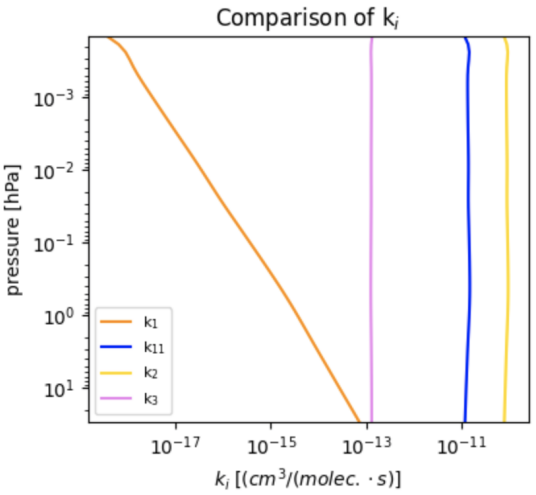

Figure 5.19: Comparison of the rate constants of all steps in the HOx/NOx cycle, excluding the photolysis reactions.

HOx/NOx/SOx cycle (see page 17)

Analogous to the HOx/NOx cycle the photolysis of NO_2 is again the rate-limiting step when only the absolute reaction rates v_i are taken into consideration, shown in figure 5.20. Therefore, the explanation of the possible connection between behaviour of the cycle and the changes in excess CO_2 would be identical as well. When alternatively looking

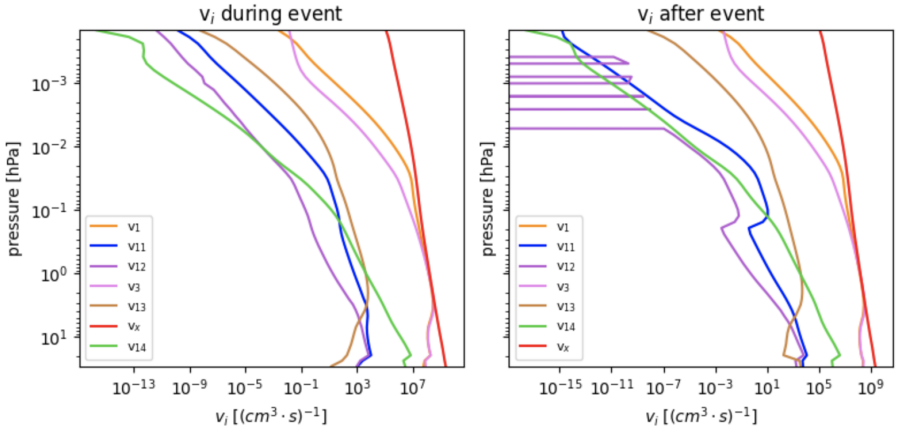

Figure 5.20: Comparison of the reaction rates v_i during and after the event of all steps in the HOx/NOx/SOx cycle, including the photolysis of CO_2 (v_x).

at the rate constants k_i again, shown in figure 5.21, then the rate-limiting step would be reaction 13 instead, which is the production of SO_3. This step shows a comparable behaviour to the reactions involved in the SOx/ClOx cycle, as can be seen in figure 5.22:

deceleration during, acceleration after the event in the pressure range $5{\times}10^{-2}$ to $1{\times}10^{0}$ hPa. Therefore, this cycle would be expected to have a similar behaviour, which can only be brought into agreement with the changes in CO_2 if a damping of the changes that are caused by the HOx cycles is assumed (meaning that if the HOx/NOx/SOx cycle would be accelerated / decelerated in the same way as the HOx cycle, the production and subsequent destruction of CO_2 would go into more extreme values).

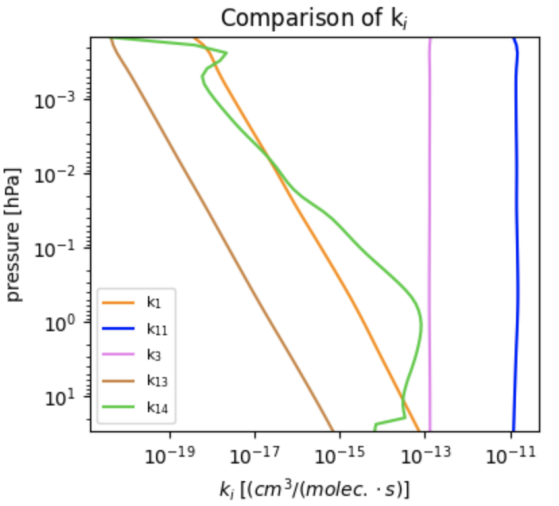

Figure 5.21: Comparison of the rate constants of all steps in the HOx/NOx/SOx cycle, excluding the photolysis reactions.

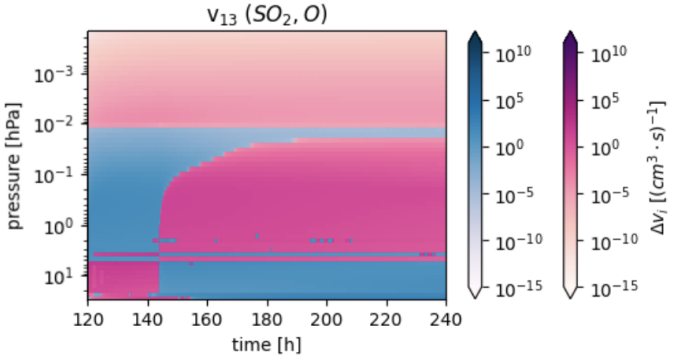

Figure 5.22: Change of the rate of reaction 13 in comparison to the reference atmosphere. Pink describes an acceleration, blue a deceleration.

5.4.3 Conclusion and outlook

As has been shown in the previous sections, the observed changes in the abundances of CO_2, CO, O_2 and O do not fit to one certain net reaction as it has been the case for the Mars simulation. This is not surprising as the cycles considered for Venus show several different net reactions that might all contribute to the changes to a certain degree, resulting in a ratio of $\Delta CO{:}\Delta O_2 > 2{:}1$.

When looking at the total reaction rates of the reactions contributing to one cycle in order to identify the rate-limiting step, the following conclusions can be drawn:

The production of a CO_2 surplus compared to the reference atmosphere during the event could be explained by the acceleration of both HOx cycles as well as of the HOx/NOx and the HOx/NOx/SOx cycle over that time interval. The contrary behaviour of the SO/ClOx cycle during the event could be expected to counteract this enhanced production, resulting in a smaller surplus than theoretically possible if all cycles were enhanced. The degradation of the excess CO_2 directly afterwards, which even turns into a deficit from day 9

on, must be explained by a strong deceleration of the catalytic cycles which only fits the behaviour of the HOx cycles. Therefore it could be assumed that their changes due to the event play the dominating role in the disturbed atmosphere, while the contrary behaviour of the other cycles has an damping effect on the destruction caused by the decelerated HOx cycles, resulting in a slower net consumption of CO_2.
However, when instead considering the rate constants k_i to identify the rate-limiting steps, the outcome of the analysis is slightly different:
The expected behaviour of the HOx cycles remains the same, as all HOx-reactions show a similar behaviour, therefore the outcome is identical regardless of which step is considered as rate-limting. Hence its behaviour still fits the observed abundance changes of CO_2 over the whole course of the simulation. The comparison of the k_i is shown in the appendix in figure 7.11, together with the respective illustration for the SOx/ClOx cycle.
is The interpretation of the HOx/NOx cycle is improving: According to the k_i the first step is the slowest, which is a HOx-reaction. This results in an expected net behaviour similar to the HOx cycles and would therefore also support the evolution of the CO_2 changes.
In the SOx/ClOx cycle, this alternative approach would switch the rate-determining step to reaction 7 instead of 9 but the two behave almost identical, as can be seen in figure 7.12 in the appendix. Consequently the cycle is expected to behave the same, too, and is still assumed to counteract the effects of the previous cycles, attenuating first the production and then the degradation of CO_2. It remains questionable to which degree this effect occurs, but this information cannot be extracted from the simulation data.
For the HOx/NOx/SOx cycle, the rate-limiting step would switch to reaction 13 instead of 12, which would result in the presumption of a temporal development similar to the SOx/ClOx cycle. Thence the only fitting interpretation would again be the inhibition of the CO_2 production during and of the destruction after the event and therefore a subordinate role of this cycle.
In conclusion it can be said that the apparent hierarchy of the cycles considered in this simulation in the disturbed atmosphere differs from the assumptions made for the quiet atmosphere. As described in section 2.2.3.2, the favored hypothesis is that the chlorine chemistry (and therefore the SOx/ClOx cycle) plays the dominating role in the CO_2 recovery, according to the research of first Yung and DeMore [27], later adopted by other scientists. The HOx and also the coupled HOx/NOx cycles on the other hand are assumed to play a subordinate role (if any), as there is no sufficient H_2O and H_2 expected in the atmosphere. The amounts of NOx necessary for the latter cycle are suspected to be probably produced by lightning, but this remained unclear. This simulation on the other hand showed that despite an under-prediction of H_2O in the atmosphere, the HOx mechanisms seemed to play the superior role in the changes of the CO_2 abundances, while especially the

SOx/ClOx cycle apparently only took a subordinate role. In general it can be concluded that the changes in the HOx budget had the most significant impact on the changes in CO_2/CO and O_2, although NOx also experienced a massive production through the event which, however, seemed to have only a minor influence on the behavior of CO_2.

Outlook

Similar to Mars, a simulation including a longer time period for the recovery of the atmosphere after the disturbance could give further insight on the longer-term behaviour of the analysed species. It could be expected that the occurring deficit of CO_2 decreases again after some time, when the deficits of especially the HOx species recover. The latter should ideally lead to an acceleration of the rate-determining steps again, decreasing the deceleration relative to the reference atmosphere and shifting the dynamical equilibrium of CO_2 again. Against the background of the transfer of H_2O into H_2, it is not guaranteed that this would indeed happen; alternatively a permanently slightly different dynamical equilibrium could be reached. As previously mentioned for Mars, an increase in simulation time is ultimately linked to an increase in computation costs and duration, therefore further limiting the analysed pressure range could be considered.

6. Assessment of errors

6.1 General remarks regarding the simulations

Ensuring mass conservation is a crucial aspect for the adequacy of a chemical model. However, due to numerical problems with the stiff differential equations it can happen that this mass conservation seems to be violated. Also at an advanced stage of this work, it turned out that the calculated changes in atomic oxygen do not completely sum up in the highest altitudes of the simulated atmospheres when the ion chemistry was used. This means that the sum of the changes of all oxygen-bearing species did not result in zero as it should (to ensure mass conservation). However, a quantitative estimate of the error revealed that the deviation relative to the values of the total oxygen (distributed across all species) is less than 0.003 %. This problem could not be solved within the scope of this work and is therefore still inherent in the analysed simulation data. One should note however that this problem only concerns pressure ranges smaller than 1×10^{-2} hPa and is therefore assumed to have no significant impact on the area focused on in this work, as its lower boundary is 5×10^{-2} hPa.
A similar problem became evident for hydrogen (at least for Venus), but primarily at the lowest levels. At pressures higher than 5×10^{0} hPa, the summed up differences of hydrogen-bearing species start to deviate from zero with the beginning of the event. In contrast to oxygen, the accumulated deviation decreases again after the end of the event simulation, but the quantitative estimation revealed a higher relative loss around 0.15 %. The reason for this remains unclear. Again, this problem concerns particularly layers outside the analysed pressure range, therefore its impact is likely to be negligible.

6.2 Venus

Two small typing errors were discovered subsequently after the end of the simulation period, which both concern implemented reactions for the Venus simulation listed previously in chapter 5.2, table 5.1. An assessment of their impact is done in the following.
In the reaction S + O_2 → SO + O, the sign in the exponent accidentally got switched (instead of $e^{\frac{100}{T}}$, $e^{\frac{-100}{T}}$ was implemented), resulting in an only slightly lower reaction rate

in the simulated pressure range. In order to assess its effects, a new reference simulation with the corrected value was made and compared to the previous reference: the results showed that the error caused only minor differences in the abundances ($\ll$ 1% change) which can be neglected, as it further did not cause any changes in the behaviour of the species that need to be considered in the analysis of the event effects.
In the reaction $SO_2 + O \xrightarrow{M} SO_3$, which is considered as a three body reaction as it needs an additional collision partner, an error was found in the exponent of the high-pressure limit taken from the JPL catalogue [34] (instead of $k_\infty^{298} = 4.1 \times 10^{-14}$, 4.1×10^{-11} was implemented). Since the pressure limit considered in the simulation is far away from the high pressure limit of the reaction (or of atmospheric gas phase reactions in general), correcting the exponent showed no change in the values of the reaction rate k in the simulated pressure range, therefore it can be expected that it had no effect on the simulation. This is further supported by the general remarks that are made in the JPL catalogue regarding the high-pressure-limit [34]: The high pressure limits of small species often lie in pressure ranges far away from values reachable in the laboratory. Therefore they are either obtained with theoretical calculations or extrapolation. The latter method results in rather inaccurate values, but as the atmospheric conditions usually lie significantly closer to the low-pressure-limit, the calculations of the rate constants are expected to be quite insensitive towards the assumed high-pressure-limits.

One further aspect that has to be considered is the scope of the implementations of the sulfur- and the extension of the chlorine chemistry, which has been limited to the neutral model. As a consequence, the new sulfur and chlorine compounds (S, SO, SO_2, SO_3, H_2SO_4, ClCO and $ClCO_3$) are not impacted by the ion chemistry directly since they are not included in that part of the model. All the changes the species experience due to the disturbance are caused by the changes in the abundances of their reaction partners due to the ion chemistry (e.g., O or O_2). It could therefore be assumed that the outcome of the simulations would be somewhat different if all these species were also taken into account in the ion chemistry model. This full implementation was not done as part of the thesis because it is much more complex and the available time period was too short for that. Nevertheless this could be especially interesting for the behaviour of the SOx/ClOx and the HOx/NOx/SOx cycle, as they both include a chlorine- or sulfur-containing rate-determining step. including a direct effect of the event on the respective species could therefore lead to major changes, particularly because HOx and NOx are already seen to experience a strong production during the event (and HOx additionally a strong degradation afterwards). If something similar happens to the SOx and ClOx species during the event, this would have a significant effect on the net behavior of the cycles, probably very

different to how they behave in this simulation.
A next step could therefore be the completion of the implementation by adding the species to the ion chemistry model and analysing its resulting impact.

7. Appendix

Mars

Simulation of the quiet atmosphere

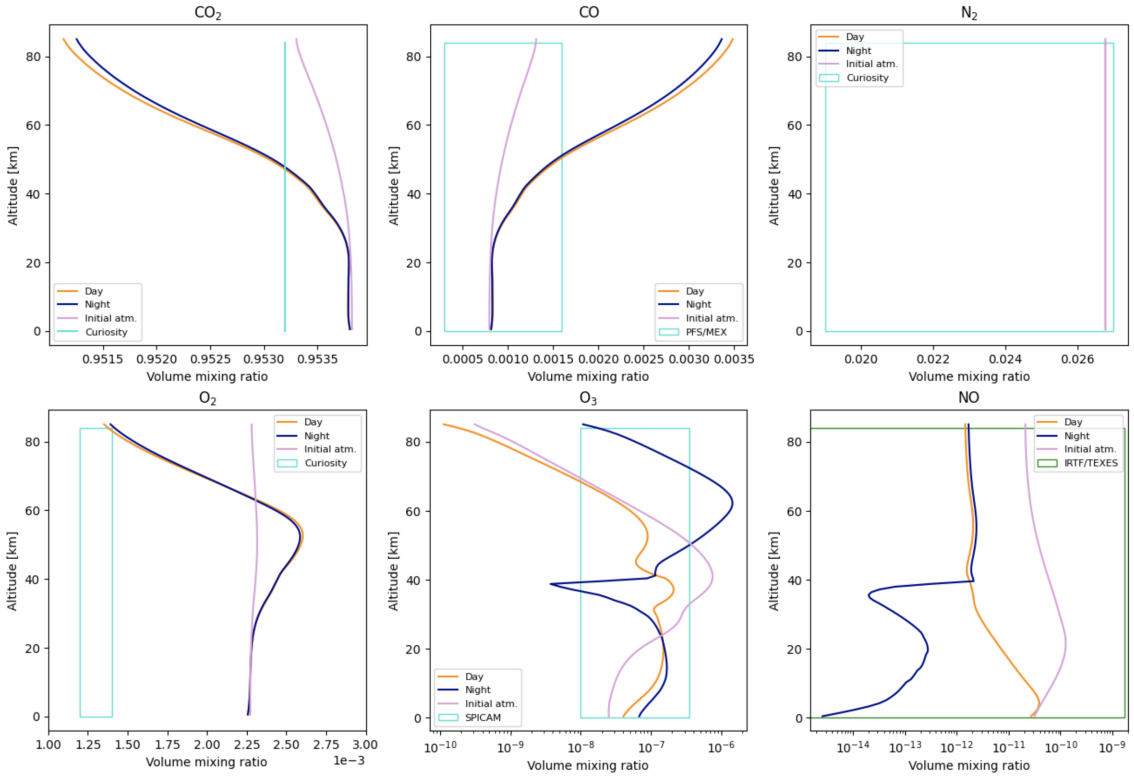

Figure 7.1: Comparison of the available measurements and the abundances resulting from the simulation for Mars. Purple shows the abundances of the initial atmosphere.

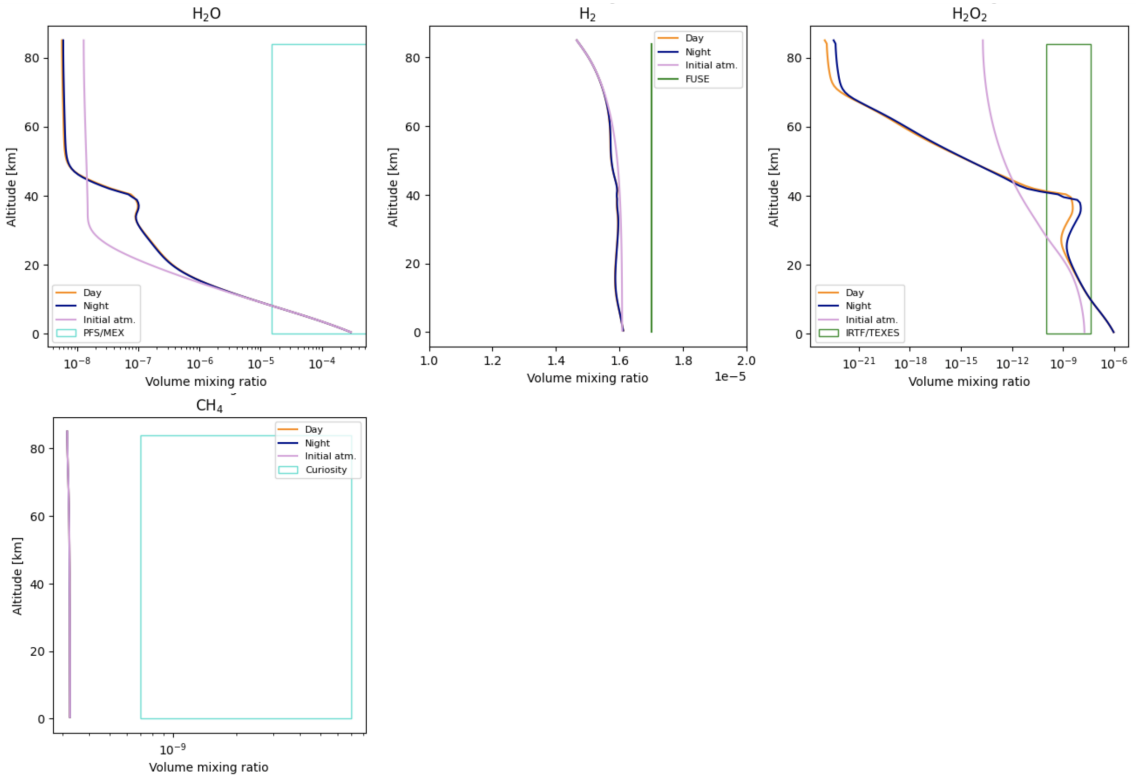

Figure 7.2: Continuation of the comparison of the available measurements and the abundances resulting from the simulation for Mars. Purple shows the abundances of the initial atmosphere.

Changes in HOx and NOx

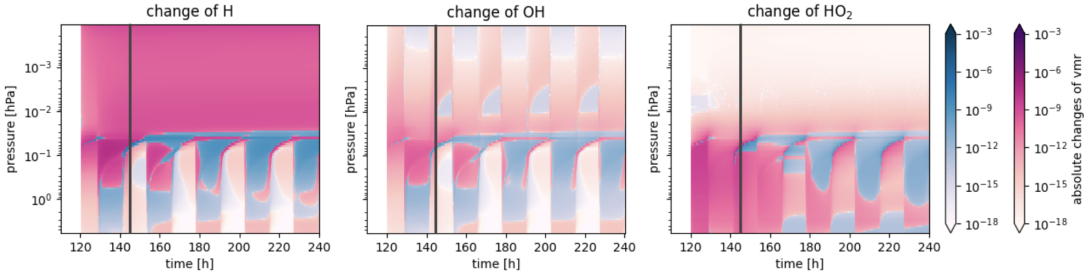

Figure 7.3: Contour plots of the changes in H, OH and HO_2 compared to the reference. Blue describes a deficit, pink a surplus in comparison to the calm atmosphere. Eventstart at night, the end of the event is marked with a grey line.

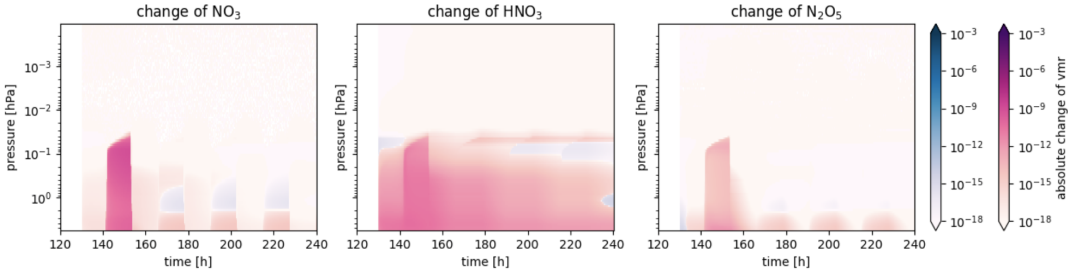

Figure 7.4: Contour plots of the changes in NO_3, HNO_3 and N_2O_5 compared to the reference. Blue describes a deficit, pink a surplus in comparison to the calm atmosphere. Eventstart during day.

Changes in CO_2, CO, O_2 and O

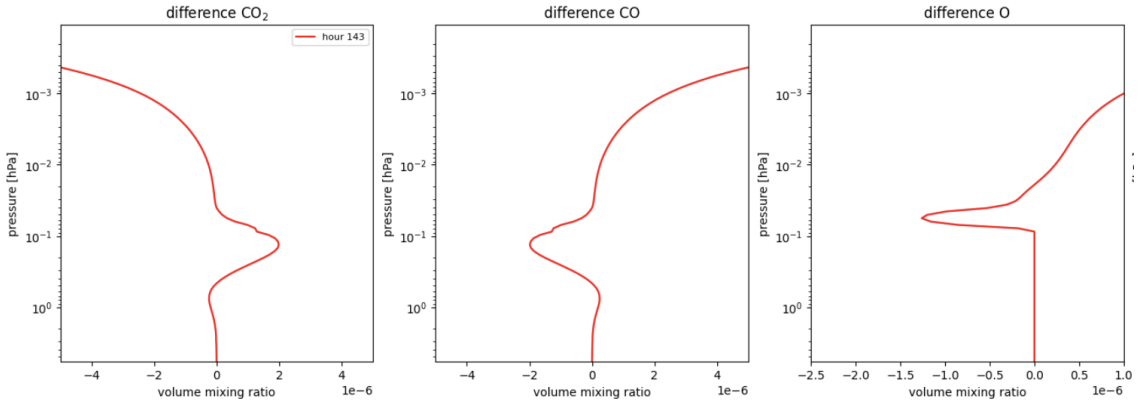

Figure 7.5: Comparison of the changes of CO_2, CO and O mid event in hour 143, shortly after sunset of day 6.

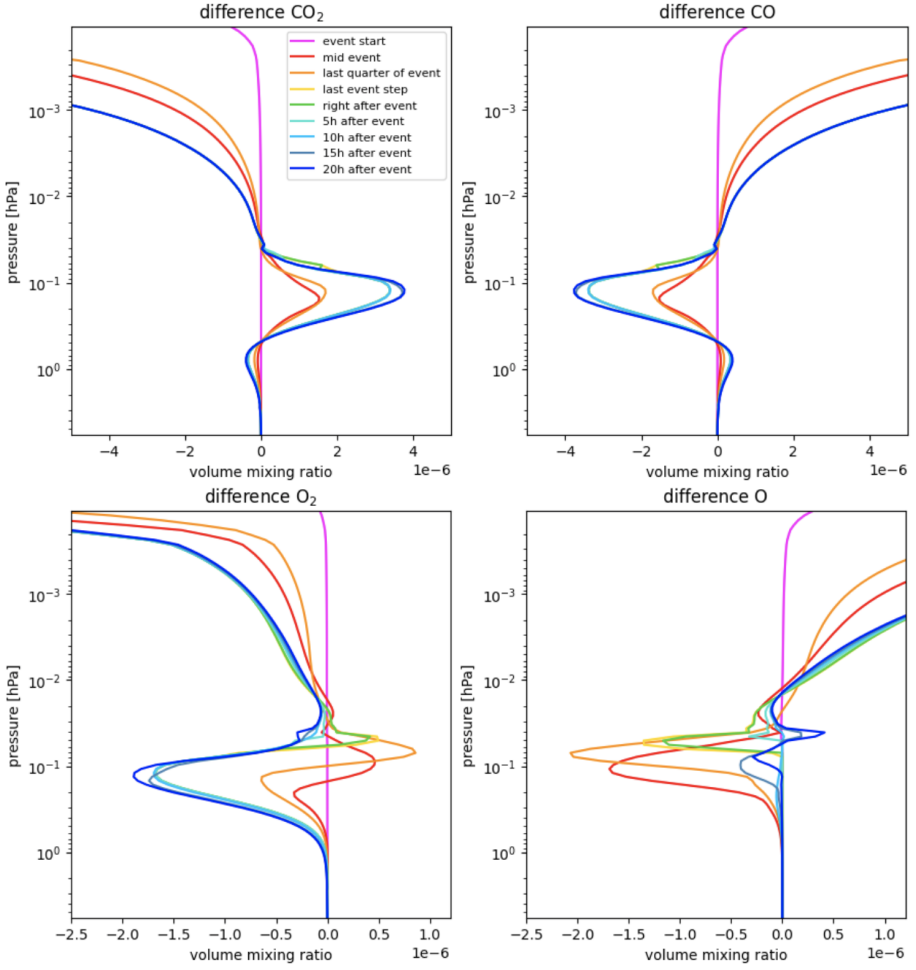

Figure 7.6: Temporal evolution of the changes in CO_2, CO, O_2 and O from the night run with focus on the event duration and the first 20 hours afterwards.

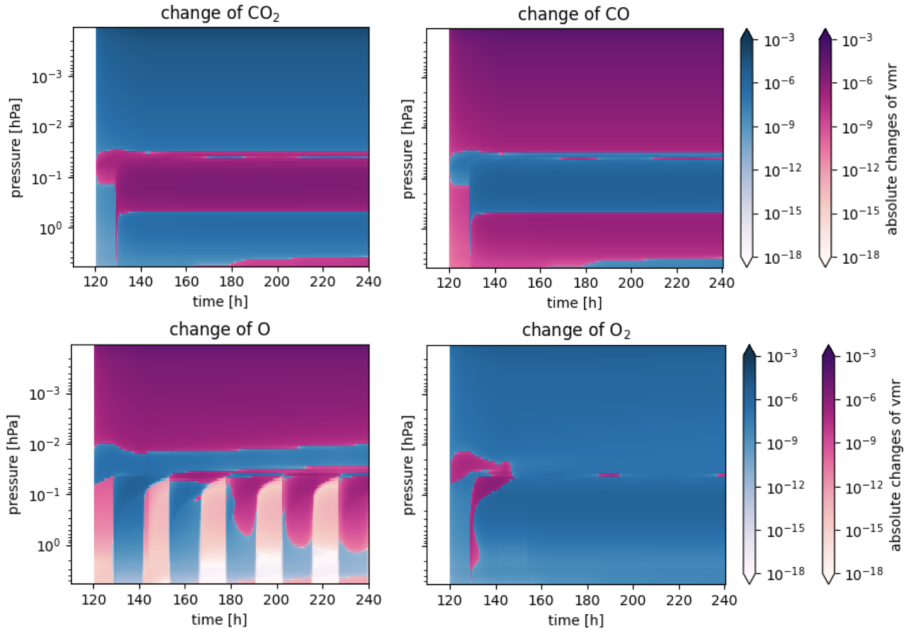

Figure 7.7: Contour plots of the changes in CO_2, CO, O and O_2 from the night run, event starting at hour 120, ending after hour 144.

Venus

Simulation of the quiet atmosphere

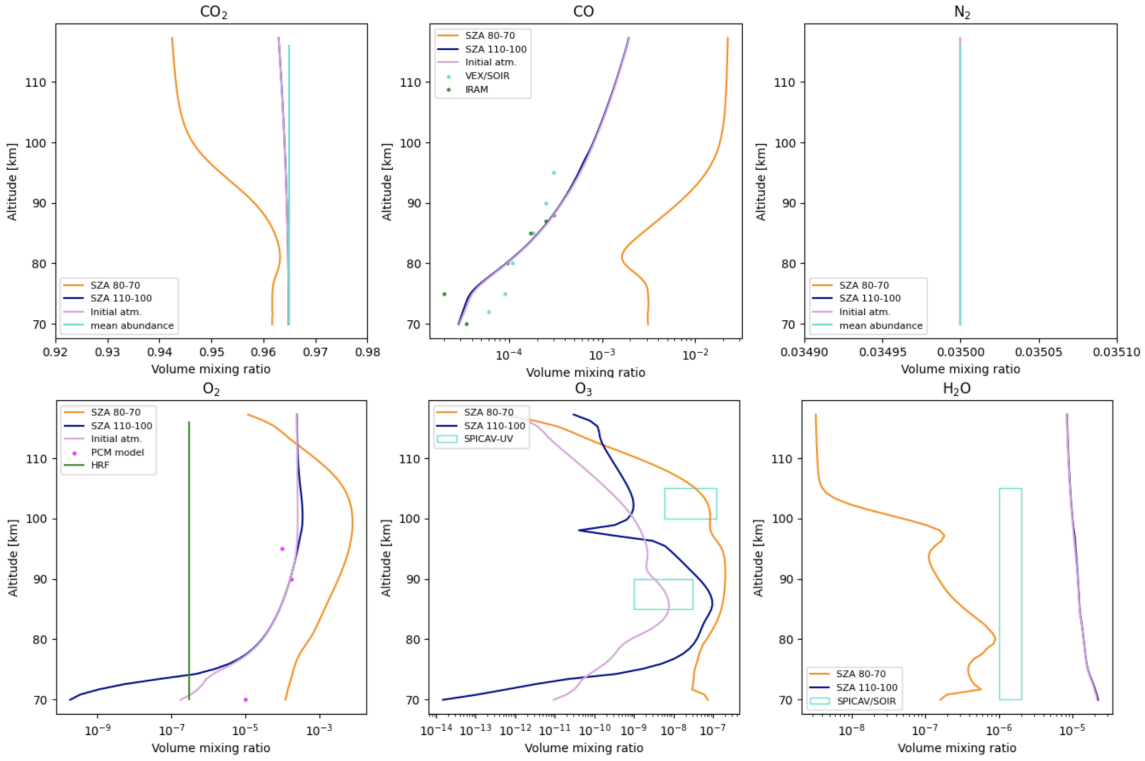

Figure 7.8: Comparison of the available measurements and the abundances resulting from the simulation for Venus. Purple shows the abundances of the initial atmosphere.

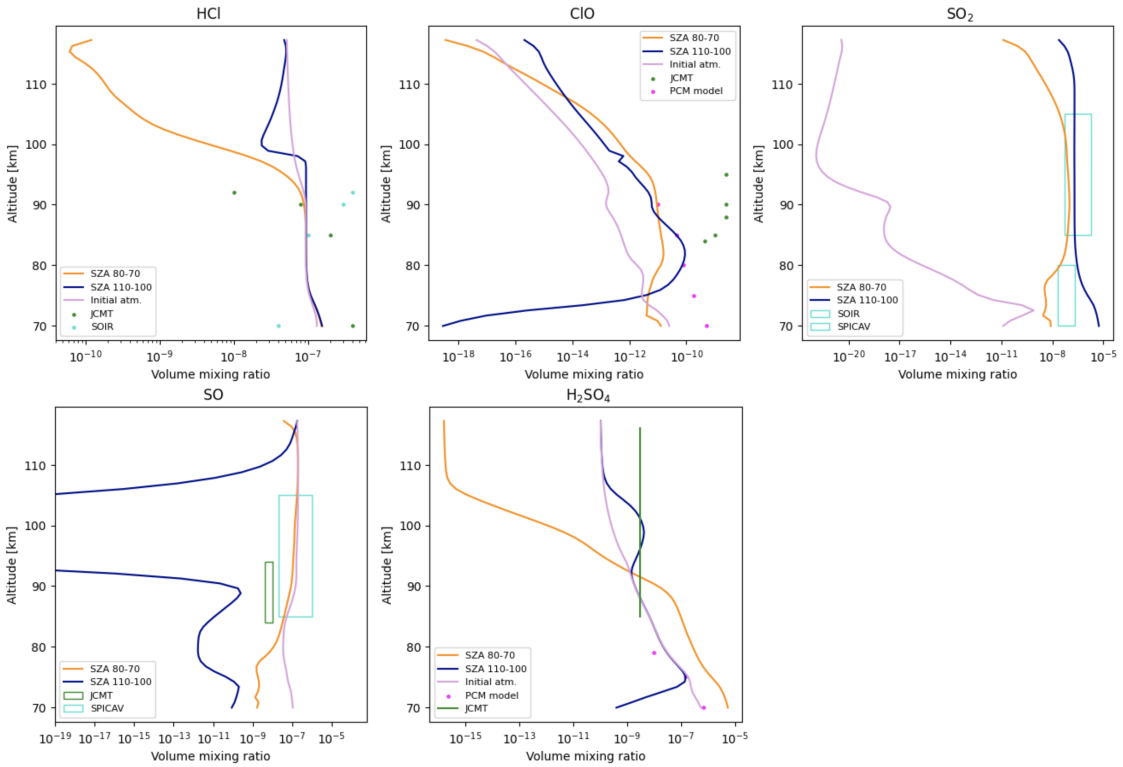

Figure 7.9: Continuation of the comparison of the available measurements and the abundances resulting from the simulation for Venus. Purple shows the abundances of the initial atmosphere.

Changes in HOx and NOx

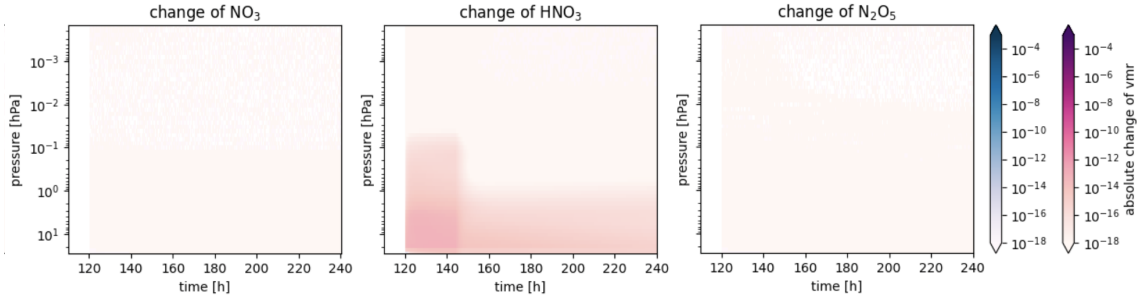

Figure 7.10: Contour plots of the changes in NO_3, HNO_3 and N_2O_5 compared to the reference for Venus. Blue describes a deficit, pink a surplus in comparison to the calm atmosphere.

Changes in the catalytic cycles

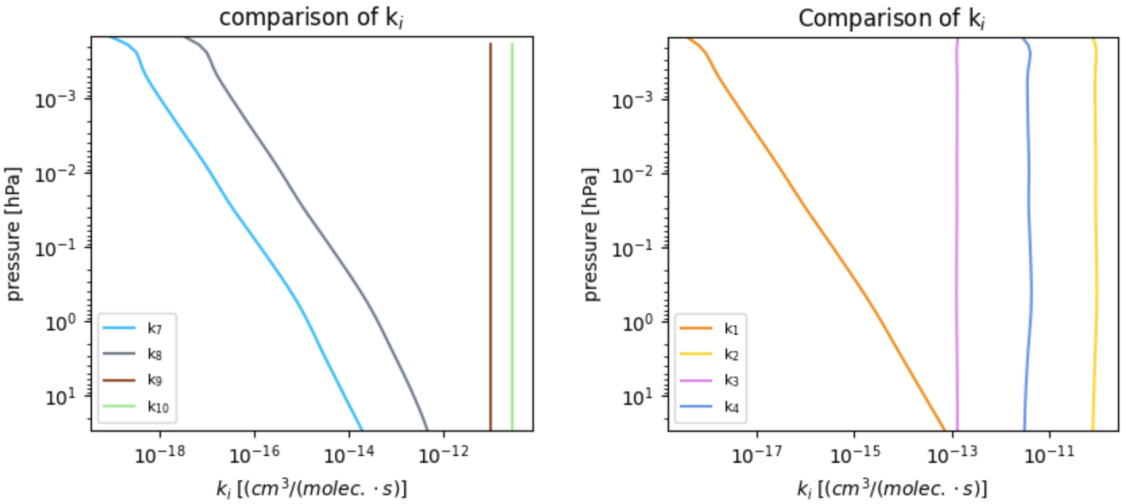

Figure 7.11: Comparison of the reaction rates k_i for the SOx/ClOx (left) and both HOx cycles (summarised in one plot, right).

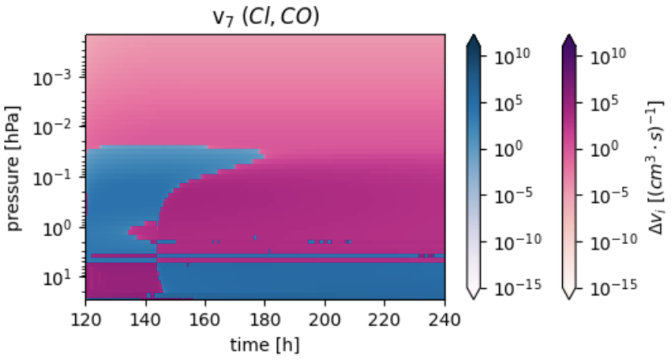

Figure 7.12: Change in the rate of v_7 in comparison to the reference atmosphere. Pink describes an acceleration, blue a deceleration.

Bibliography

[1] V. Bozza, L. Mancini, A. Sozzetti, editors, *Astrophysics of Exoplanetary Atmospheres*, Springer International Publishing AG, 1. edition, **2018**.

[2] K. Vida, Z. Kővári, A. Pál, K. Oláh, L. Kriskovics, *The Astrophysical Journal*, **2017**, *841*, 124.

[3] V. Bothmer, I. Daglis, *Space Weather - Physics and Effects*, Springer Verlag Berlin Heidelberg, publushed in association vith Praxis Publishing Ltd, 1. edition, **2007**.

[4] I. de Pater, J. J. Lissauer, *Planetary Sciences*, Cambridge University Press, 2. edition, **2015**.

[5] M. Sinnhuber, H. Nieder, N. Wieters, *Surveys in Geophysics*, **2012**, *33*, 1281–1334.

[6] D. J. Jacob, *Introduction to Atmospheric Chemistry*, Princeton University Press, Princeton, **2000**.

[7] C. H. Jackman, M. T. DeLand, G. J. Labow, E. L. Fleming, D. K. Weisenstein, M. K. W. Ko, M. Sinnhuber, J. M. Russell, *Journal of Geophysical Research: Space Physics*, **2005**, *110*.

[8] H. Nieder, *Modellstudien zur Untersuchung des Einflusses solarer Prozesse auf die mittlere Atmosphäre*, Dissertation, Karlsruher Institut für Technologie, **2015**.

[9] Dr. David R. Williams, NASA Goddard Space Flight Center, Planetary fact sheets, **2016**, accessed: 2024-07-07.

[10] E. F. Milone, W. J. Wilson, *Solar System Astrophysics - Planetary Atmospheres and the Outer Solar System*, Springer New York, NY, **2014**.

[11] R. M. Haberle, R. T. Clancy, F. Forget, M. D. Smith, R. W. Zurek, *The Atmosphere and Climate of Mars*, Cambridge University Press, **2017**.

[12] R. P. Wayne, *Chemistry of Atmospheres*, Oxford University Press, 3. edition, **2000**.

[13] A. Määttänen, F. Lefèvre, L. Verdier, F. Montmessin, C. Listowski, S. Guilbon, A. Fedorova, O. Korablev, *Icarus*, **2022**, *387*, 115162.

[14] Paul R. Mahaffy et al., *Science*, **2013**, *341*, 263–266.

[15] C. R. Webster, P. R. Mahaffy, S. K. Atreya, G. J. Flesch, M. A. Mischna, P.-Y. Meslin, K. A. Farley, P. G. Conrad, L. E. Christensen, A. A. Pavlov, J. Martín-Torres, M.-P. Zorzano, T. H. McConnochie, T. Owen, J. L. Eigenbrode, D. P. Glavin, A. Steele, C. A. Malespin, P. D. Archer, B. Sutter, P. Coll, C. Freissinet, C. P. McKay, J. E. Moores, S. P. Schwenzer, J. C. Bridges, R. Navarro-Gonzalez, R. Gellert, M. T. Lemmon, the MSL Science Team, *Science*, **2015**, *347*, 415–417.

[16] G. Sindoni, V. Formisano, A. Geminale, *Planetary and Space Science*, **2011**, *59*, 149–162.

[17] D. D. Bogard, D. H. Garrison, J. Masarik, *Meteoritics & Planetary Science*, **2001**, *36*, 107–122.

[18] S. Perrier, J. L. Bertaux, F. Lefèvre, S. Lebonnois, O. Korablev, A. Fedorova, F. Montmessin, *Journal of Geophysical Research: Planets*, **2006**, *111*.

[19] T. Encrenaz, B. Bézard, T. Greathouse, M. Richter, J. Lacy, S. Atreya, A. Wong, S. Lebonnois, F. Lefèvre, F. Forget, *Icarus*, **2004**, *170*, 424–429.

[20] V. A. Krasnopolsky, P. D. Feldman, *Science*, **2001**, *294*, 1914–1917.

[21] A. Stolzenbach, F. Lefèvre, S. Lebonnois, A. Määttänen, *Icarus*, **2023**, *395*, 115447.

[22] A. Vandaele, A. Mahieux, S. Chamberlain, B. Ristic, S. Robert, I. Thomas, L. Trompet, V. Wilquet, J. Bertaux, *Icarus*, **2016**, *272*, 48–59.

[23] D. A. Belyaev, F. Montmessin, J.-L. Bertaux, A. Mahieux, A. A. Fedorova, O. I. Korablev, E. Marcq, Y. L. Yung, X. Zhang, *Icarus*, **2012**, *217*, 740–751.

[24] B. J. Sandor, R. Todd Clancy, G. Moriarty-Schieven, F. P. Mills, *Icarus*, **2010**, *208*, 49–60.

[25] Y. L. Yung, W. B. DeMore, *Photochemistry of Planetary Atmospheres*, Oxford University Press, **1999**.

[26] M. B. McElroy, N. D. Sze, Y. L. Yung, *Journal of Atmospheric Sciences*, **1973**, *30*, 1437 – 1447.

[27] Y. L. Yung, W. DeMore, *Icarus*, **1982**, *51*, 199–247.

[28] A. J. Watson, T. M. Donahue, D. H. Stedman, R. G. Knollenberg, B. Ragent, J. Blamont, *Geophysical Research Letters*, **1979**, *6*, 743–746.

[29] W. Chameides, J. Walker, A. Nagy, *Nature*, **1979**, *280*, 820–822.

[30] E. Marcq, F. P. Mills, C. D. Parkinson, A. C. Vandaele, *Space Science Reviews*, **2018**, *214*.

[31] P. W. Atkins, *Physikalische Chemie*, Wiley-VCH, Weinheim, Germany, 6. edition, **2022**.

[32] M. P. Chipperfield, *Journal of Geophysical Research: Atmospheres*, **1999**, *104*, 1781–1805.

[33] S. P. Sander, R. R. Friedl, A. R. Ravishankara, D. M. Golden, C. E. Kolb, M. J. Kurylo, M. J. Molina, G. K. Moortgat, B. J. Finlayson-Pitts, P. H. Wine, R. E. Huie, **2006**, *JPL Publication 06-2*.

[34] J. B. Burkholder, S. P. Sander, J. Abbatt, J. R. Barker, C. Cappa, J. D. Crounse, T. S. Dibble, R. E. Huie, C. E. Kolb, M. J. Kurylo, V. L. Orkin, C. J. Percival, D. M. Wilmouth, P. H. Wine, **2019**, *JPL Publication 19-5*.

[35] F. Wunderlich, M. Scheucher, M. Godolt, J. Grenfell, F. Schreier, P. Schneider, D. Wilson, A. Sànchez-Lopèz, M. Pòpez-Puertas, H. Rauer, *ApJ*, **2020**, *901*.

[36] K. Herbst, J. L. Grenfell, M. Sinnhuber, H. Rauer, B. Heber, S. Banjac, M. Scheucher, V. Schmidt, S. Gebauer, R. Lehmann, F. Schreier, *AA*, **2019**, *631*, A101.

[37] R. R. A. Ramaroson, *Modélisation locale, à une et trois dimensions des processus photochimiques de l'atmosphère moyenne*, Thesis, Université Pierre et Marie Curie - Paris VI, **1989**.

[38] H. Winkler, *The response of middle atmospheric ozone to solar proton events in a changing geomagnetic field*, Dissertation, Universität Bremen, **2008**.

[39] V. A. Krasnopolsky, *Icarus*, **2006**, *182*, 80–91.

[40] V. A. Krasnopolsky, *Icarus*, **2012**, *218*, 230–246.

[41] J. C. Miller, R. J. Gordon, *The Journal of Chemical Physics*, **12 1981**, *75*, 5305–5310.

[42] D. Freeman, K. Yoshino, J. Esmond, W. Parkinson, *Planetary and Space Science*, **1984**, *32*, 1125–1134.

[43] V. Prahlad, S. Ahmed, V. Kumar, *Journal of Quantitative Spectroscopy and Radiative Transfer*, **1996**, *56*, 57–66.

[44] C. Robert Wu, B. Yang, F. Chen, D. Judge, J. Caldwell, L. Trafton, *Icarus*, **2000**, *145*, 289–296.

[45] K. Bogumil, J. Orphal, T. Homann, S. Voigt, P. Spietz, O. Fleischmann, A. Vogel, M. Hartmann, H. Kromminga, H. Bovensmann, J. Frerick, J. Burrows, *Journal of Photochemistry and Photobiology A: Chemistry*, **2003**, *157*, 167–184.

[46] L. F. Phillips, *J. Phys. Chem.*, **1981**, *85*, 3994–4000.

[47] M. J. Mills, O. B. Toon, V. Vaida, P. E. Hintze, H. G. Kjaergaard, D. P. Schofield, T. W. Robinson, *Journal of Geophysical Research: Atmospheres*, **2005**, *110*.

[48] J. B. Burkholder, M. Mills, S. McKeen, *Geophysical Research Letters*, **2000**, *27*, 2493–2496.